JOURNAL OF GEOPHYSICAL RESEARCH, VOL. 106, NO. B12, PAGES 30,475–30,504, DECEMBER 10, 2001

Rapid active thrusting along the northwestern range front of the Tanghe Nan Shan (western Gansu, China)

J. Van der Woerd,[1,2] Xu Xiwei,[3] Li Haibing,[4] P. Tapponnier,[2]
B. Meyer,[2] F. J. Ryerson,[1] A.-S. Meriaux,[2] and Xu Zhiqin [4]

Abstract. The western part of the Tanghe Nan Shan range southwest of Subei (western Gansu, China) is presently growing on thrust ramps splaying from the left-lateral Altyn Tagh Fault. Late Cenozoic thrusting has folded and sliced Oligocene-Miocence red beds into an imbricate wedge, capped by warped and uplifted Quaternary terraces that form a 2- to 5-km-wide ledge, north of the steeply faceted range front. Seismic scarps 1.5 to 4.5 m high cut young fans along the outer thrusts. Carbon 14 dating of organic remains collected on strath terraces constrains the chronology of deposition and incision by the streams. Most of the fans and terraces in the southern part of the Subei basin appear to have been emplaced after the last glacial maximum, particularly during the early Holocene optimum (9-5 ka). Measurements of the shapes of the warped terraces constrain minimum and maximum throws on the outer thrusts. The minimum vertical throw of 34 ± 2 m of a surface dated at 8411 ± 530 years B.P. at one site provides a minimum vertical uplift rate of 4.1 ± 0.5 mm/yr. The maximum possible uplift (115 ± 15 m) of the oldest terrace surface, whose probable age is 15 to 18 ka, places an upper bound on the uplift rate of 7 ± 2 mm/yr. The thrust geometry at depth and the cumulative shortening (10-20 km) deduced from balancing sections logged across the imbricate thrust wedge are consistent with a shortening rate of about 5 mm/yr and an onset of thrusting at about 4 ± 2 Ma. Such a shortening rate implies a significant northward decrease in slip rate along the Altyn Tagh Fault. The recent growth of the western Qilian mountain ranges thus appears to be intimately coupled with sinistral motion on the Altyn Tagh Fault and the extrusion of Tibet.

1. Introduction

The large NW-SE trending ranges located north of the Qaidam basin, between the Altyn Tagh and Haiyuan faults (Figure 1) [*Tapponnier and Molnar*, 1977], have been interpreted to grow as ramp anticlines on active thrusts of crustal scale [*Tapponnier et al.*, 1990; *Meyer*, 1991; *Meyer et al.*, 1998]. The regional northeastward elevation decrease (~3000 m to 1200 m above sea level (asl)) and the fact that such ranges terminate on the Altyn Tagh Fault suggest a close relationship between sinistral faulting and thrusting [*Peltzer et al.*, 1988; *Meyer et al.*, 1998; *Métivier et al.*, 1998]. The 300-km-long Tanghe Nan Shan, west of Hala Hu Lake, is one of the highest such ranges (5500 m asl; Figure 1). The Paleozoic core of the range overthrusts folded Oligocene-Miocene red beds [*Regional Geology of Gansu Province*, 1989; *Bohlin*, 1937]. The most prominent thrusts dip south, folding and cutting coalescent Quaternary fans that mantle the northern foreland of the range. Topographic and geomorphic comparisons with the next range to the north (Daxue Shan) [*Tapponnier et al.*, 1990; *Meyer et al.*, 1998] suggest uplift and shortening rates of millimeters per year.

Over a distance of 50 km, the Tanghe Nan range, whose average trend is ~N125°E, veers counterclockwise toward the northwest, to become roughly parallel with the N70°E striking Altyn Tagh Fault (Figure 1). The northern, principal branch of the fault keeps striking N70°E across the Subei basin [*Tapponnier et al.*, 1990; *Ge et al.*, 1992; *Meyer et al.*, 1996], while the main Tanghe Nan Shan frontal thrusts splay from it toward the southeast (Figure 1). To the southwest, the southern branch of the fault follows the curved axis of the range (Figure 1). Such relationships between the sinistral faults, the range, and the thrust imply that a fraction of the strike-slip displacement is locally trans-

[1]Lawrence Livermore National Laboratory, Livermore, California, USA.
[2]Institut de Physique du Globe de Paris, Paris, France.
[3]China Seismological Bureau, Beijing, China.
[4]Institute of Geology, Ministry of Land and Resources, Beijing, China.

Copyright by the American Geophysical Union.

Paper number 2001JB000583.
0148-0227/01/2001JB000583$09.00

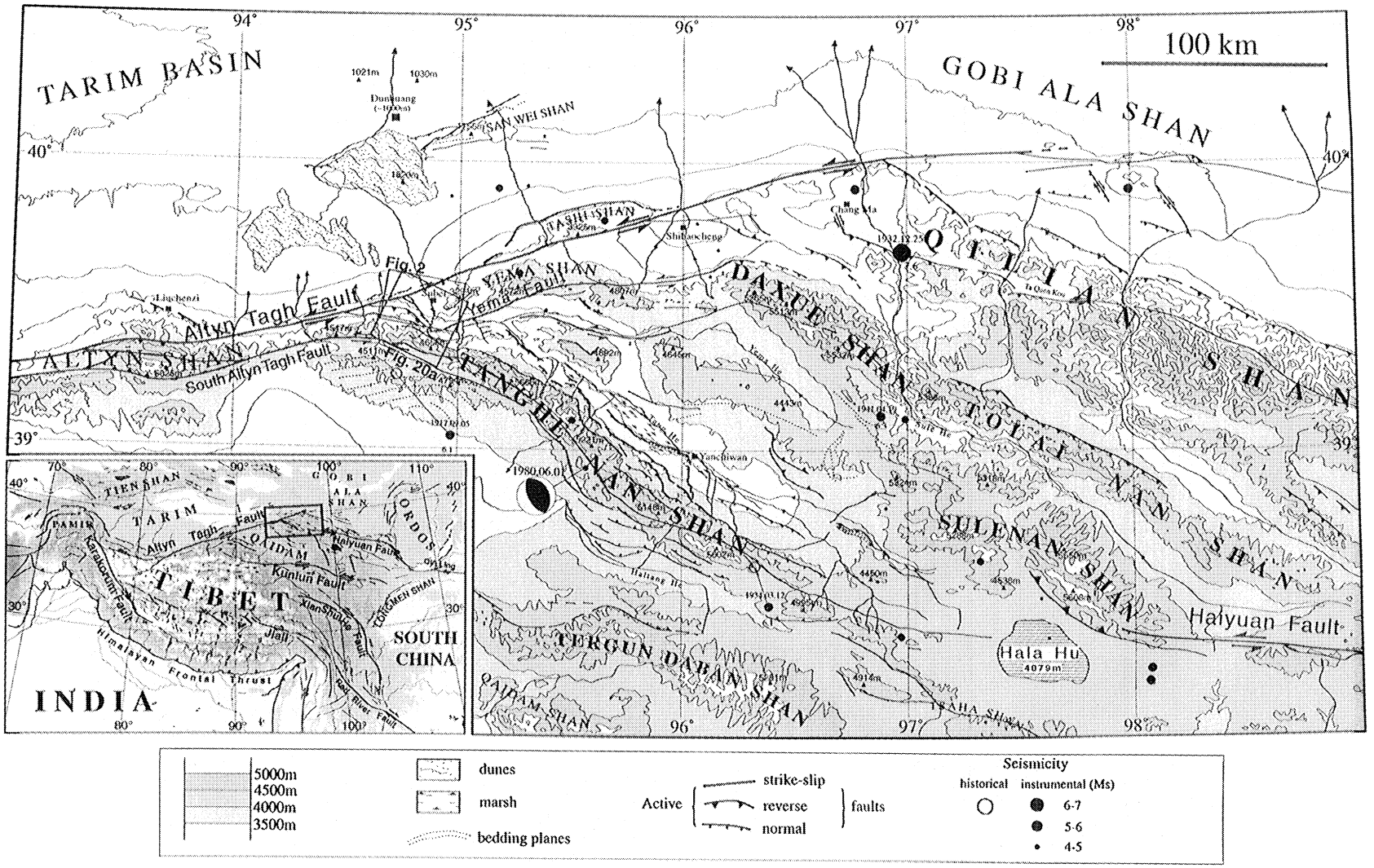

Figure 1. Seismotectonic map of the northeast corner of Tibet (modified from *Tapponnier et al.* [1990] and *Meyer et al.* [1998]). Note linear N70°E striking left-lateral Altyn Tagh Fault at western terminations of Qilian, Daxue, and Tanghe Nan Shan. N120°E striking Tanghe Nan Shan veers counterclockwise to WSW before meeting with Altyn Tagh Fault west of Subei. About five earthquakes with magnitude between 5 and 6.1 occurred along Tanghe Nan Shan since 1960. Fault plane solution for one event is from *Molnar and Lyon-Caen* [1989]. The nodal planes strike parallel to the range, compatible with north vergent thrust [e.g., *Meyer*, 1991]. Inset is location of figure within Asia.

formed into thrusting, folding, and mountain building. Southeast of Subei, the Tanghe Nan Shan frontal thrust trace steps ~25 km northeastward across the sinistral Yema Fault (Figure 1). Thrusting continues at least 150 km farther southeastward along the south side of the Yanchiwan basin [*Meyer et al.*, 1998] (Figure 1). All along the northern piedmont of the range, Oligocene-Miocene red beds, as well as recent Quaternary terraces that unconformably cap them (e.g., Figure 2 and Plate 1) are folded and uplifted by active north vergent thrusts. These observations are not consistent with the interpretation of *Wang* [1997], who failed to identify the main active trace of the Altyn Tagh Fault across the Subei basin and inferred that the fault had cut and displaced already folded Tertiary rocks.

In order to quantitatively constrain shortening across the Tanghe Nan Shan, we carried out a detailed field study of the range front southwest of Subei. Our geomorphic and geological mapping of the largest recent and active features was based on the combined analysis of SPOT images, air photos, topographic maps (1:100,000 and 1:50,000 scale), and sections logged in the field. The maps and sections were used to constrain the deep geometry of the thrusts and to estimate amounts of finite shortening [e.g., *Avouac et al.*, 1993; *Meyer et al.*, 1998]. Total station leveling of folded and uplifted ^{14}C-dated alluvial terraces provided bounds on vertical throw, river incision, and shortening rates.

2. Folding and Uplift Along the Northwestern Piedmont of the Tanghe Nan Shan

2.1. Quaternary Deposits in and Around Subei Basin

The small Subei basin lies about 2100 m asl, between the Tanghe Nan and Yema Shan. Fed by glacial meltwaters from the Tanghe Nan and Daxue Shan, the Tanghe River, largest permanent river to flow out of the Tibetan highlands between 90°E and 96°E, crosses the basin (Figures 1 and 2). Cultivated fields are restricted to the terraces of that river. The rest of the region is a desert and most other streams are intermittent, with small springs locally watering patches of grass.

We used two SPOT images, one multispectral (KJ237-271, Figure 2), the other panchromatic (KJ236-271), with ground resolutions of 20 m and 10 m, respectively, to identify active faults and map recent geological and geomorphic units (Plate 1). The relative chronology of Quaternary terraces and fans was defined on the basis of height, degree of incision, and loess cover thickness. Five main terrace and fan levels may thus be regionally correlated (Figure 2 and Plate 1). Such deposits are not uniformly distributed across the Subei basin, which is asymmetric. The oldest terraces and fans (T4 and T5, Plate 1) cover large areas north of Subei. They are extensively covered with thick loess. T5 is preserved mostly north of the Altyn Tagh Fault (Plate 1). South of Subei, on top of an uplifted ledge between the two principal thrusts (F0 and F1-F2, Plate 1 and Figure 3), terrace fanglomerates form strath deposits up to several meters thick. They unconformably cap folded Oligocene-Miocene red sandstones and conglomerates. Downstream from the northern thrust (F1-F2), large fans are made of thicker accumulations of conglomerates.

The main level (T3) capping the red beds on the ledge at the foot of the range (Plate 1 and Figure 3) is uniformly uplifted, warped, and folded by F1-F2. It is especially well preserved east of stream r7, where the range front is steeper, and along Xishui Gou (r8 in Plate 1), where it correlates with a broad level in the upper catchment. We thus infer that T3 was emplaced in a relatively short period of time, when the streams had enough power to abrade the red beds and reshape the upper part of the piedmont. Across the ledge between F0 and F1-F2, two principal inset strath terrace levels (T2, T1) are limited to small elongated patches, mapped in detail along r5 and r6 (Plate 1). T2 also floors a broad, abandoned channel on the left side of r8, south of F3 (Plate 1).

The fans north of thrusts F1-F2-F3 probably formed coevally with the terrace deposits in the middle reach of the streams. But while uplift due to thrusting preserved older units on the hanging wall, younger deposits cover older ones on the footwall. Tongues of f2-f1 fans appear to form most of the depositional surface (bajada) north of the thrusts (Figures 2 and 3 and Plate 1), the largest and longest one being that abandoned by r8 west of its present course (Plate 1). The oldest fans (f3 and f4) are preserved west of that tongue north of the Altyn Tagh Fault, probably because they escaped being covered by younger deposits owing to offset and capture (Plate 1)[*Van der Woerd*, 1998].

The overall emplacement pattern and relative chronology of the youngest alluvial deposits (T1-T3) prompt the following inferences. The distribution of the terrace levels suggests a regional abrasion-deposition event (T3) followed by smaller, episodic aggradation within the stream channels (T1, T2). As confirmed below by absolute dating, such changes in the stream regimes appear to be of climatic origin, with the regional event occurring in tune with deglaciation and subsequent events modulated by minor climatic changes during the Holocene, a situation similar to that encountered elsewhere in Asia [e.g., *Peltzer et al.*, 1988; *Tapponnier et al.*, 1990; *Gaudemer et al.*, 1995; *Lasserre et al.*, 1999] and demonstrated along the Kunlun Fault to the southeast [*Van Der Woerd et al.*, 1998].

2.2. Geometry of Cenozoic Folding and Thrusting Southwest of Subei

The terraces incised downslope from the range front southwest of Subei imply uplift of the 3- to 4-km-

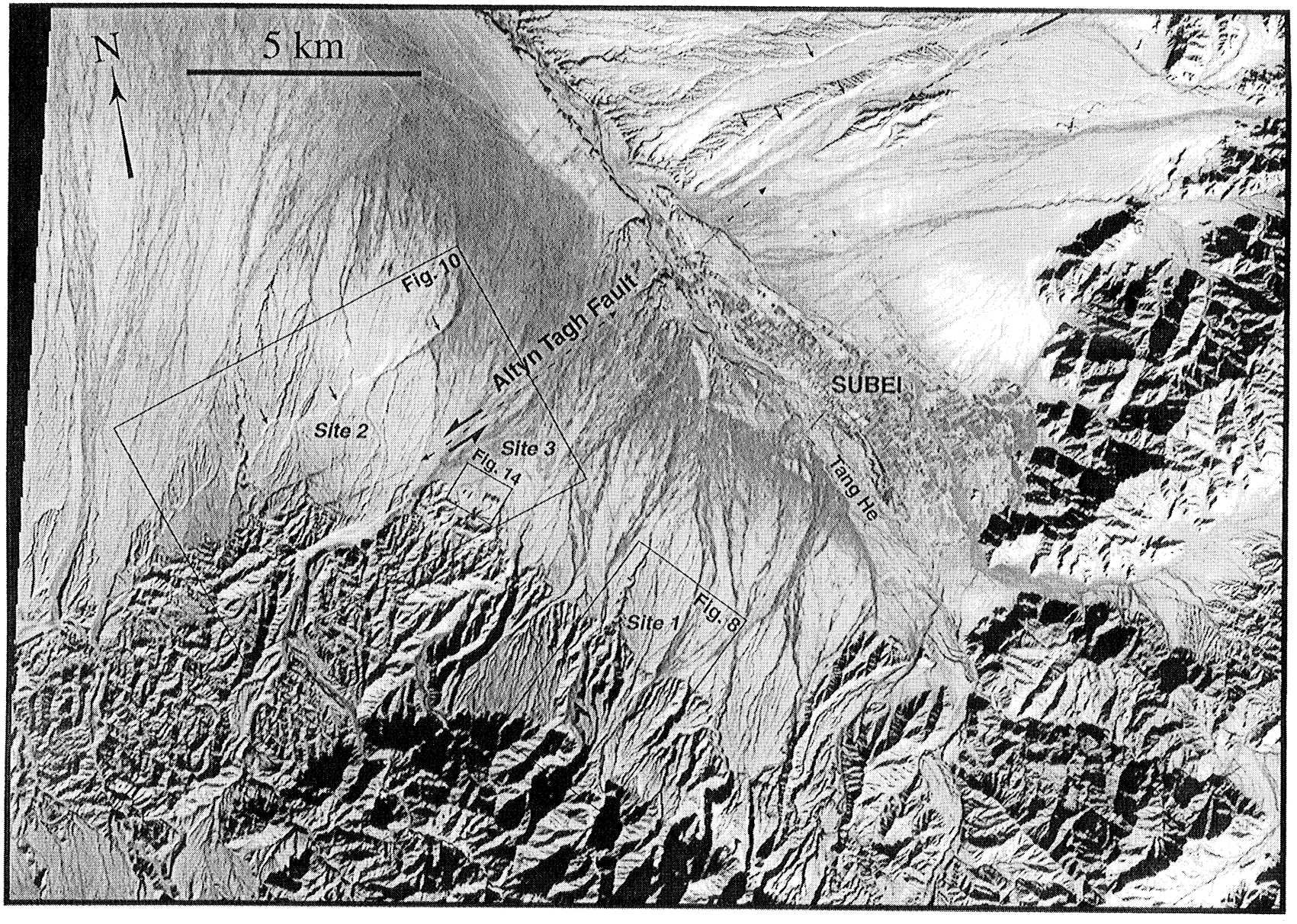

Figure 2. Multispectral SPOT image (KJ237-271) of Subei basin. Subei village is located on right bank of Tanghe River. Basin is limited to southwest by Tanghe Nan Shan thrust and to northwest by active left-lateral Altyn Tagh Fault. North of Altyn Tagh Fault, en échelon, south facing scarps (sunlit, arrows) reflect normal faulting.

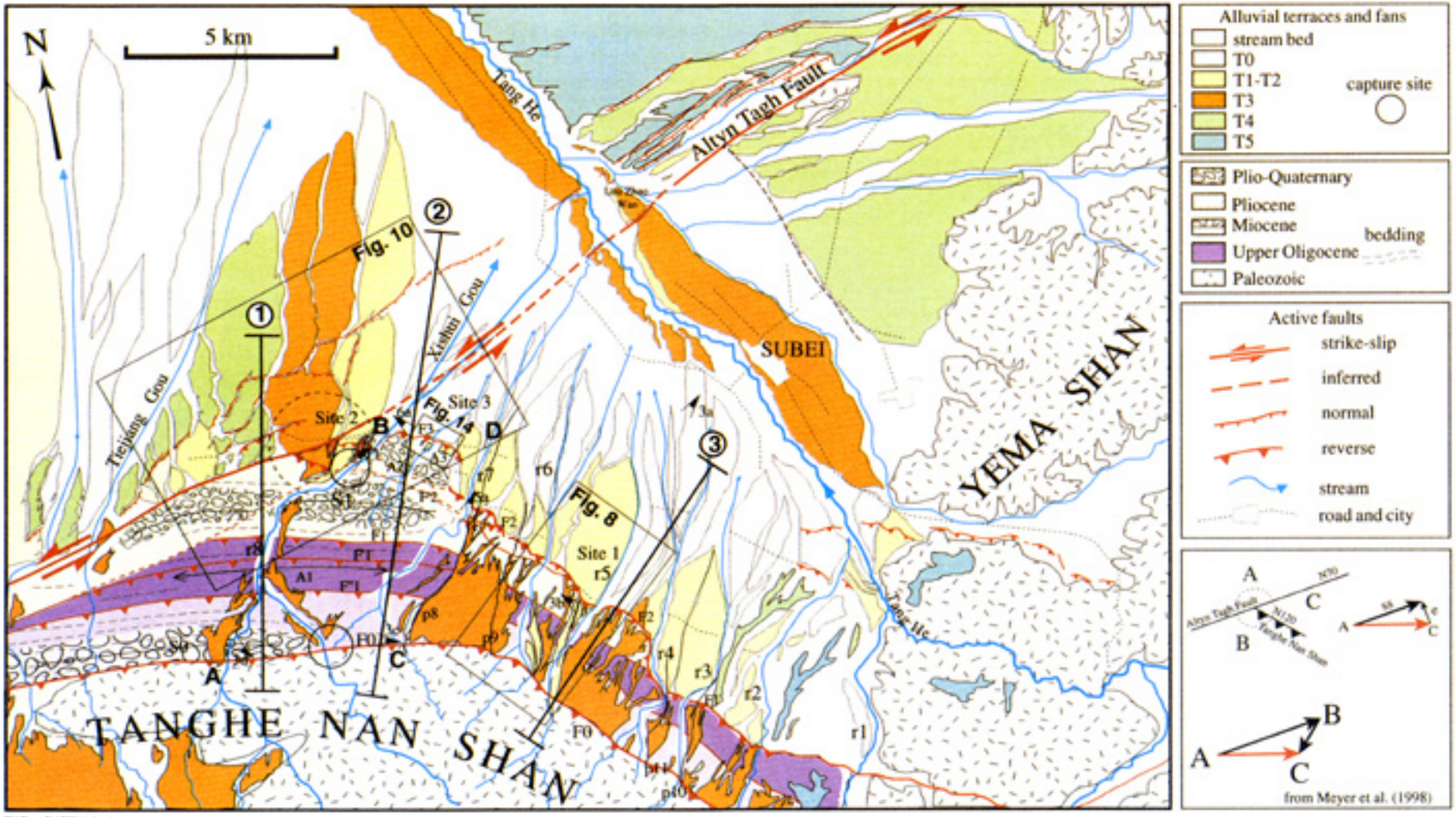

Plate 1. Geomorphic and tectonic interpretation of Figure 2. AB and CD are sections logged in the field along streambed Xishui Gou (r8) and r7, respectively (see Figure 4); 1, 2 and 3 are synthetic sections a, b, and c, respectively, of Figure 7. Terraces and fans chronologies are from SPOT analysis, field observations, and ^{14}C dating (see text). Circles indicate capture sites: past (to the north) and future (to the south) of stream r8 by stream r7.

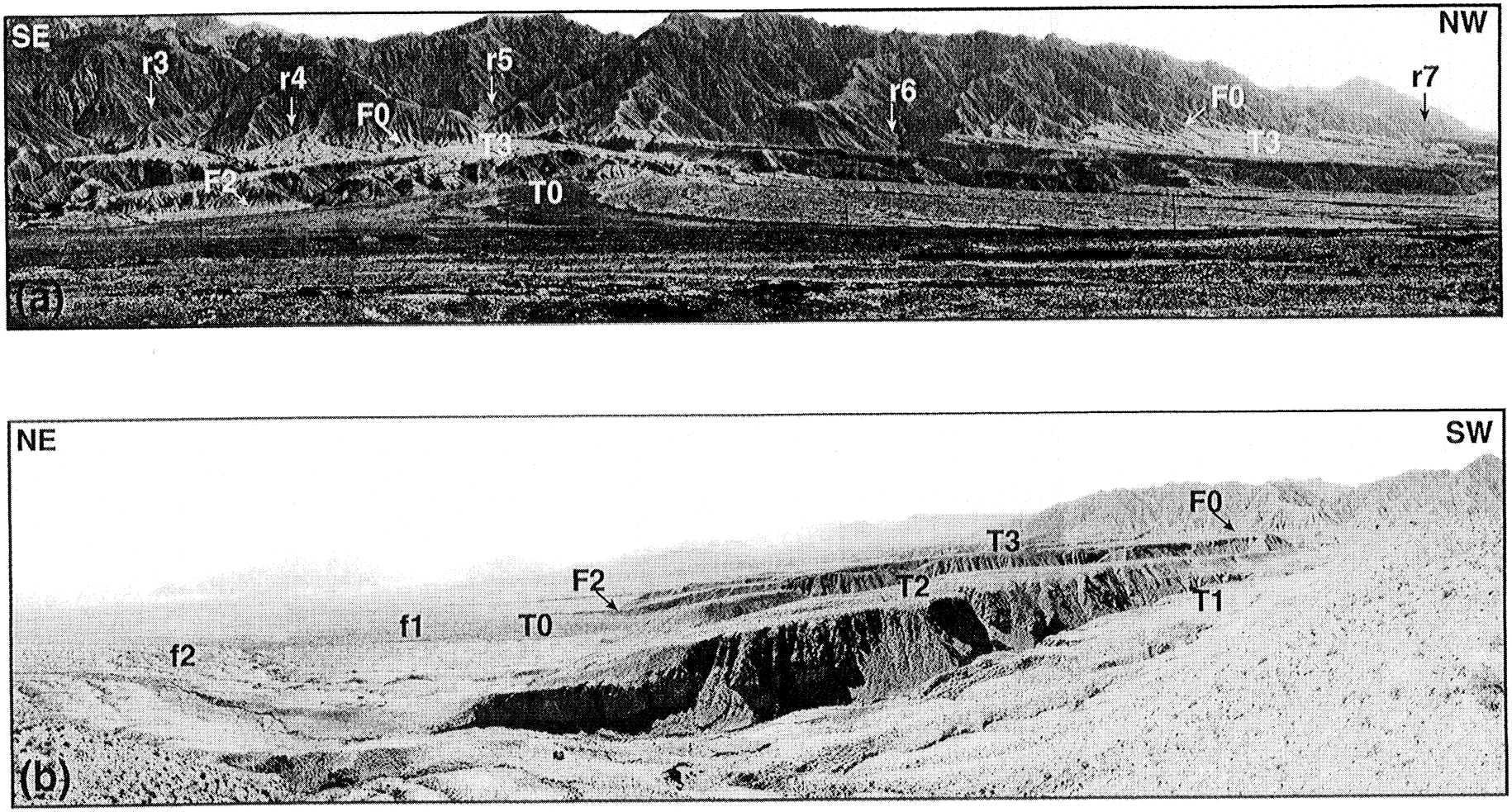

Figure 3. (a) View to the southwest of faulted and uplifted piedmont south of Subei. T3 upper terrace level extends regionally in front of Tanghe Nan Shan. (b) View to east across folded thrust front at site 1 near stream r5. Alluvial terraces T3, T2, and T1 are made of meters thick conglomerates that lie unconformably on south dipping Oligocene-Miocene red beds. Steep forelimb of anticline is due to flexural folding of terraces above ramp F2.

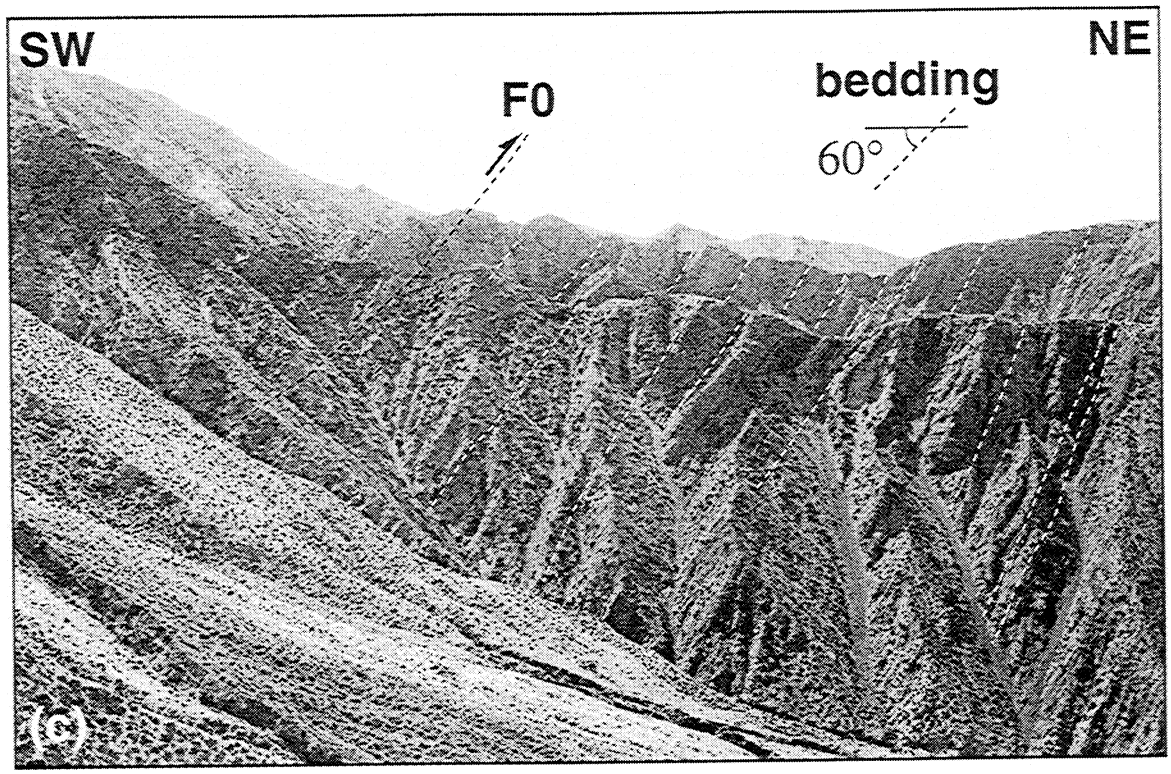

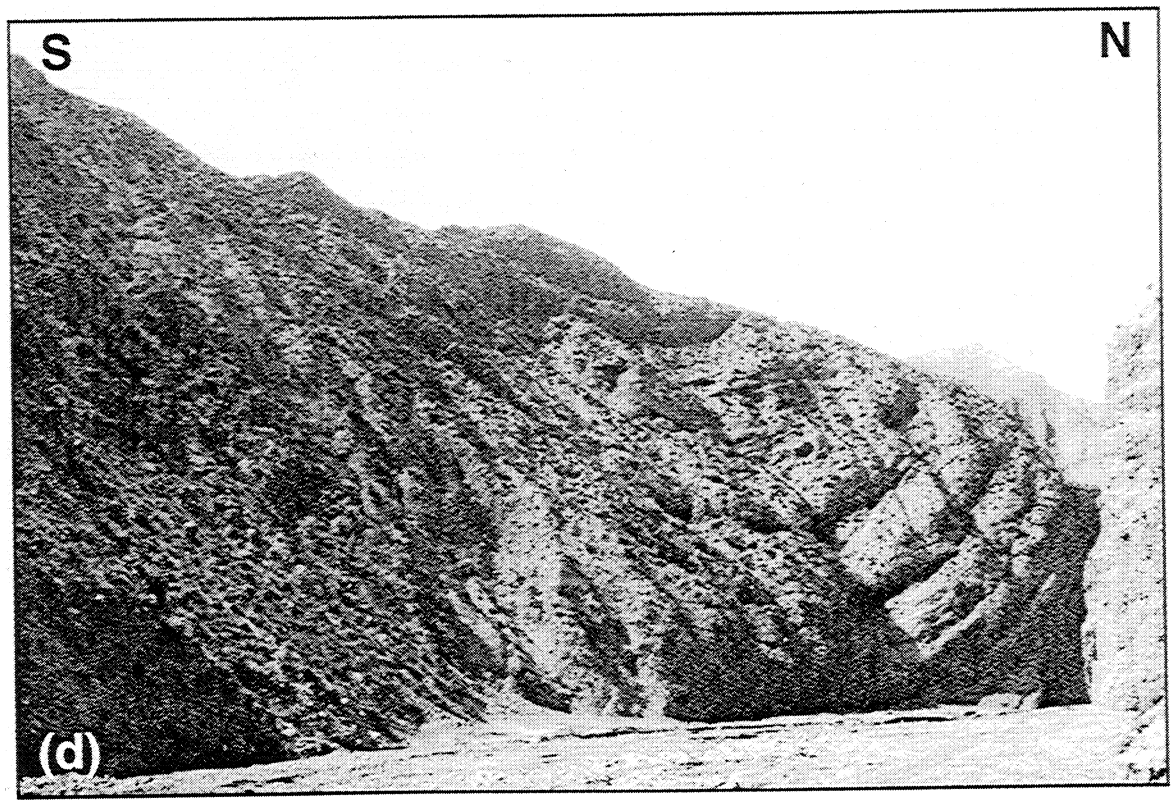

Figure 3. (continued) (c) View to the north of Paleozoic-Tertiary tectonic contact along r7. Steep thrust F0 has same dip as red sandstones. (d) Syncline S0 along stream r8 with rounded cobbles up to 50 cm in diameter, north of F0.

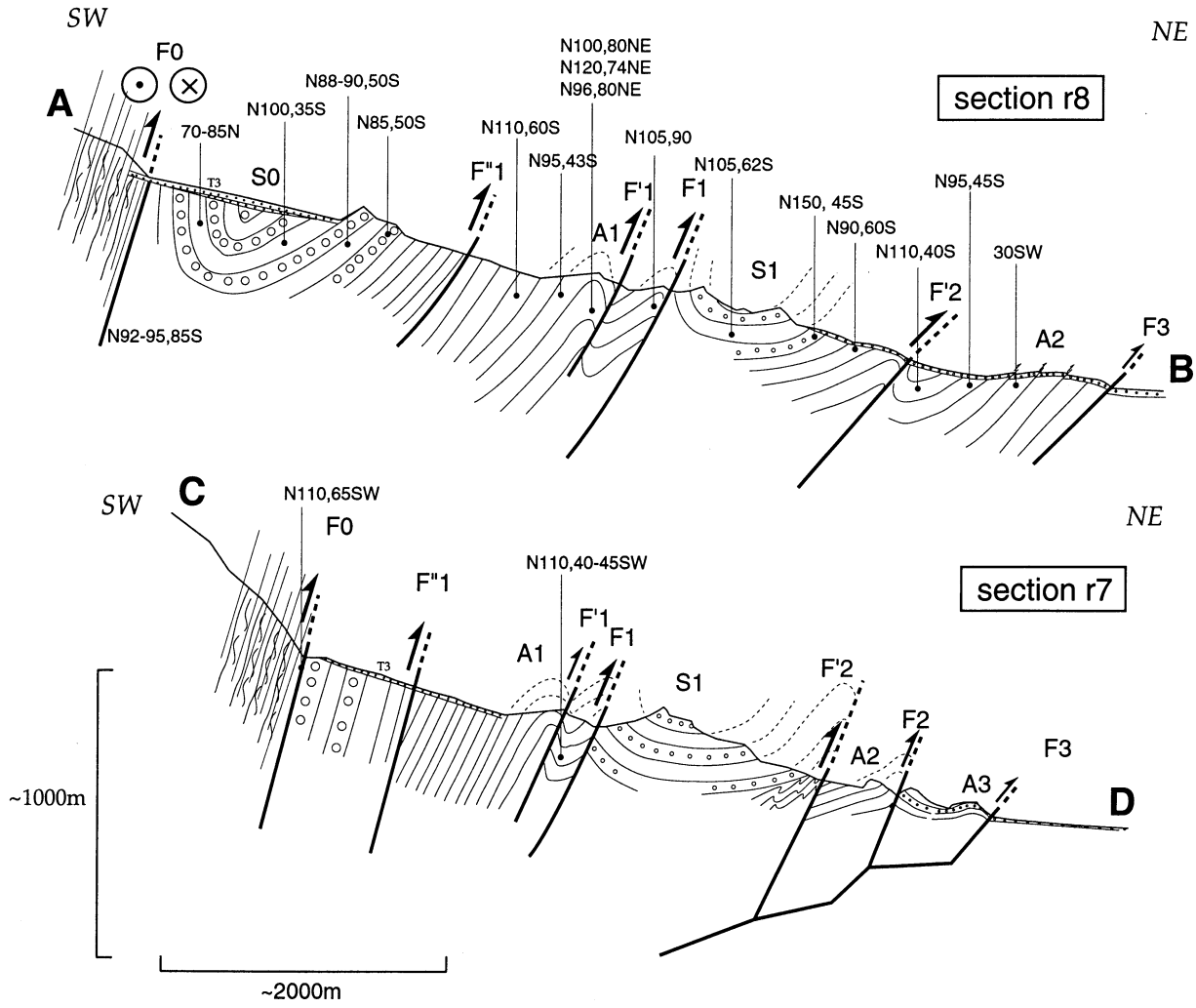

Figure 4. Field cross sections along streams r8 and r7, AB and CD, respectively, in Plate 1. Main thrusts can be traced from one section to the next.

wide ledge between F0 and F1-F2 (Plate 1 and Figure 3). Thrusting and folding are well exposed in the red beds north of the faceted spurs cut into the Paleozoic metavolcanic greenschists that form the uplifted basement of the range (Figure 2). The thrusts and folds extend from the Altyn Tagh Fault to the southeast corner of the Subei basin. A lobate, north facing cumulative flexural scarp outlines the outer piedmont thrusts (F1, F2, and F3; Plate 1 and Figure 3). This scarp strikes N100°-N115°E close to the fault and N135°E farther away. The shape of the scarp and of the flexed, uplifted terraces south of it (Figure 3b) are characteristic of a fold growing above a thrust ramp [e.g., *Suppe*, 1983; *Tapponnier et al.*, 1990; *Meyer et al.*, 1998]. South of the piedmont thrust, the range front thrust (F0, Figure 3c) curves more progressively toward the Altyn Tagh Fault (Plate 1).

Two sections along canyons cut by streams r7 and r8 (Plate 1 and Figure 4) expose the imbricate structure of the fold and thrust zone between the range front (F0) and piedmont thrusts (F2, F3; Figures 3c and 4). Despite lateral variations and the westward widening of this imbricate thrust wedge, both sections show similar overall geometry. On the longest, Xishui Gou section (r8), several south dipping thrusts (F′0, F′1, F1, F′2, F2) slice the wedge, separating red bed units with average dips of ~50°-60° SW (Figures 3 and 4). The section starts at the front of the range with a tight syncline (S0) of massive, competent conglomerates with intervening red horizons, which pinches out toward the east (Figures 3d and 4). At the base of the facets, the range front thrust (F0) brings foliated, steeply south dipping greenschists, on top of thick, steeply south dipping beds of grey and purplish sandstones (Figures 3c and 4). To the west, F0 strikes N95°E, dips 85°S, and exhibits nearly horizontal slickensides. It is sealed by colluvial conglomerates with angular pebbles that form the base of T3. To the east, by contrast, past the bend across r6, where it veers to a ~N135°E strike, F0 is less steep and still absorbs, with predominantly dip-slip motion, a fraction of the present-day shortening. About 3.5 km down section, F1, marked by sheared rocks, thrusts folded, deep

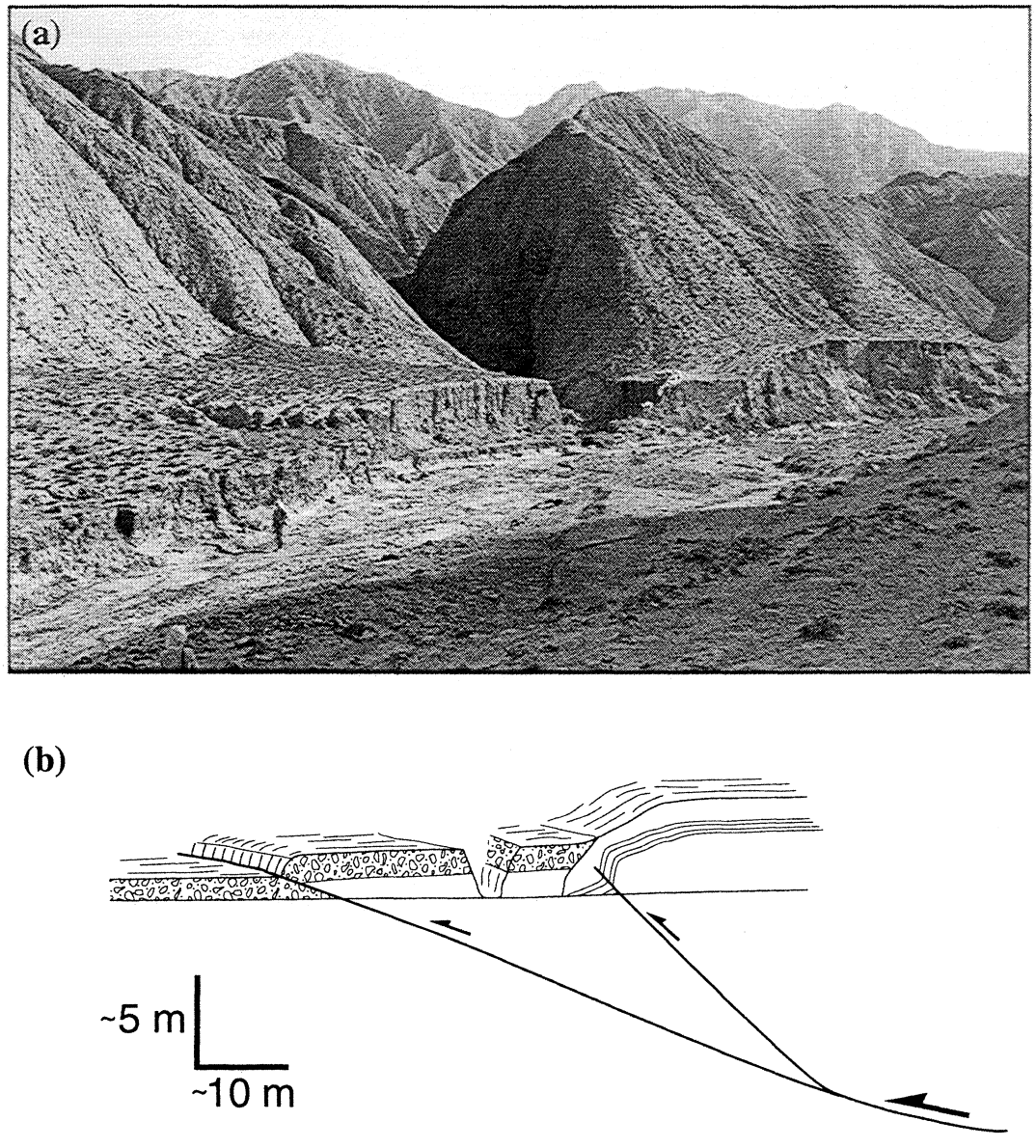

Figure 5. (a) Seismic scarp across a recent terrace of stream r7, ~200 m southwest of F2. Southwest view is of scarp (black arrows) across terrace and fold (white arrow) with clear overturned alluvial layers unconformably covered by more recent terrace deposits. (b) Schematic interpretation of scarp and fold geometry associated with thrust propagation.

red to purple sandstones onto a ~1-km-wide "piggyback" syncline (S1, Figure 4) of gray conglomerates. Farther down, these conglomerates and the conformable red beds underneath are thrust by F′2 onto the light orange to pink mudstones of the foremost Neogene unit. On the south limb of A2, near the piedmont thrust, the base of T′3 is offset by bedding slip (Figure 4).

Along r7, ~1 km south of the frontal thrust (F2), a free-faced, ~2-m-high seismic scarp offsets the lowest terrace and lateral colluvial fans on its top (Figure 5). Twenty meters upstream, the incised bank exposes folded mudstones and gravels in the hanging wall of another small thrust that has uplifted this terrace (Figure 5). Both probably merge at depth (Figure 5b), as commonly observed [e.g., *Tapponnier et al.*, 1990; *Avouac et al.*, 1993; *Meyer et al.*, 1998; *Avouac et al.*, 1992; *Stein and Ekström*, 1992]. The foremost frontal thrusts on this section are thus seismically active.

Between r7 and r8, dome-shaped hills made of folded Quaternary fanglomerates (A3, site 2, Figures 2, 4, and 6 and Plate 1) reflect the growth of an asymmetric anticline, whose steeper northern limb is bounded by seismic thrust scarplets (Figure 6b), marking the emergence of the thrust ramp farthest from the range (F3) and closest to the Altyn Tagh Fault.

The deeply incised wedge of red beds capped by warped and uplifted Quaternary conglomerates thus appears to have grown through the unabated, foreland mi-

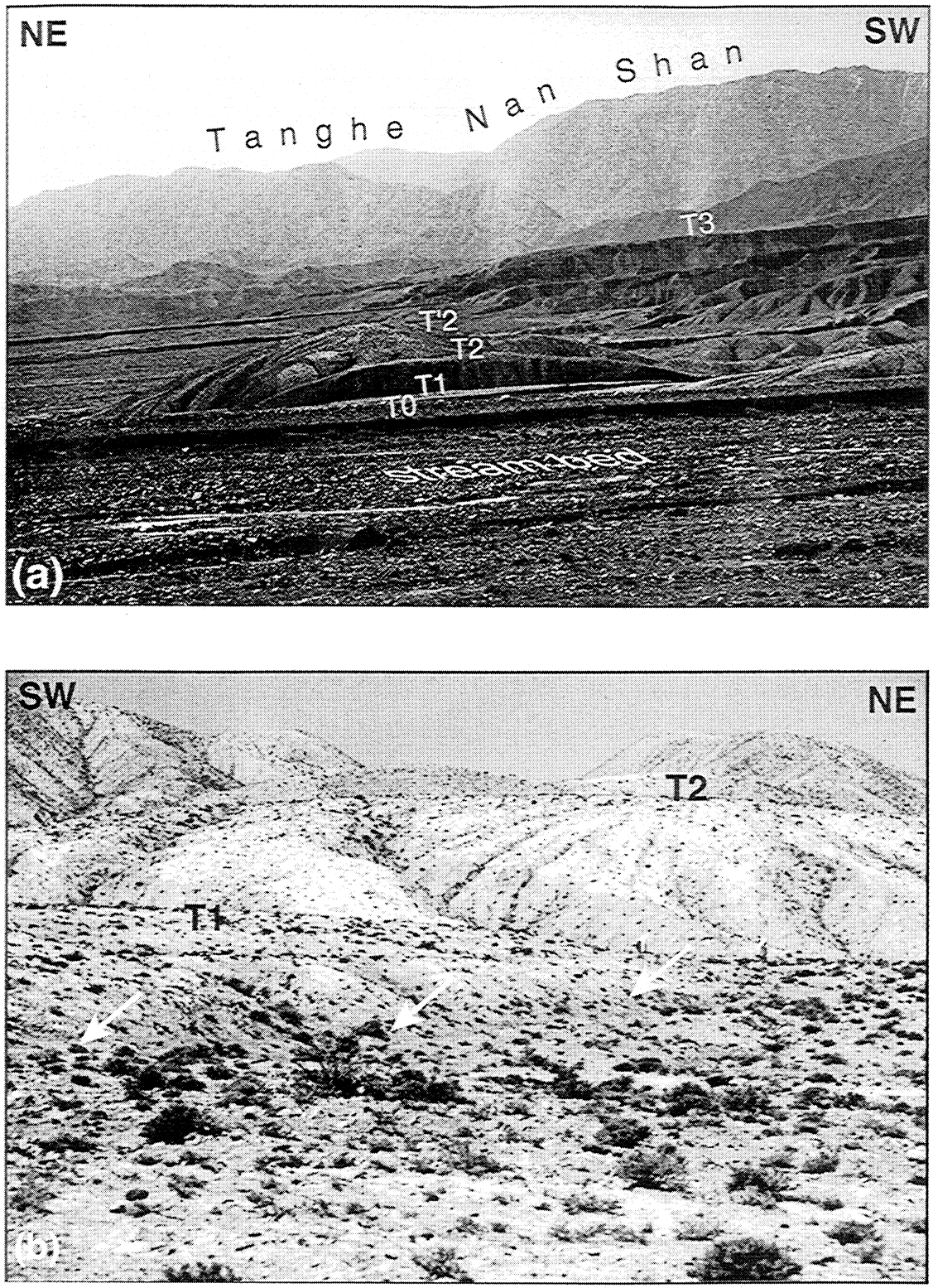

Figure 6. (a) View, to the south, of anticline A3, foremost growing fold above southwest dipping thrust ramp (F3). Larger flexure in the background is capped by terrace T3. (b) Scarp, 1 to 2 m high, of thrust F3, due to recent earthquake, offsets young terrace T1. Note rounded, eroded riser of T2 and deeply incised gullies.

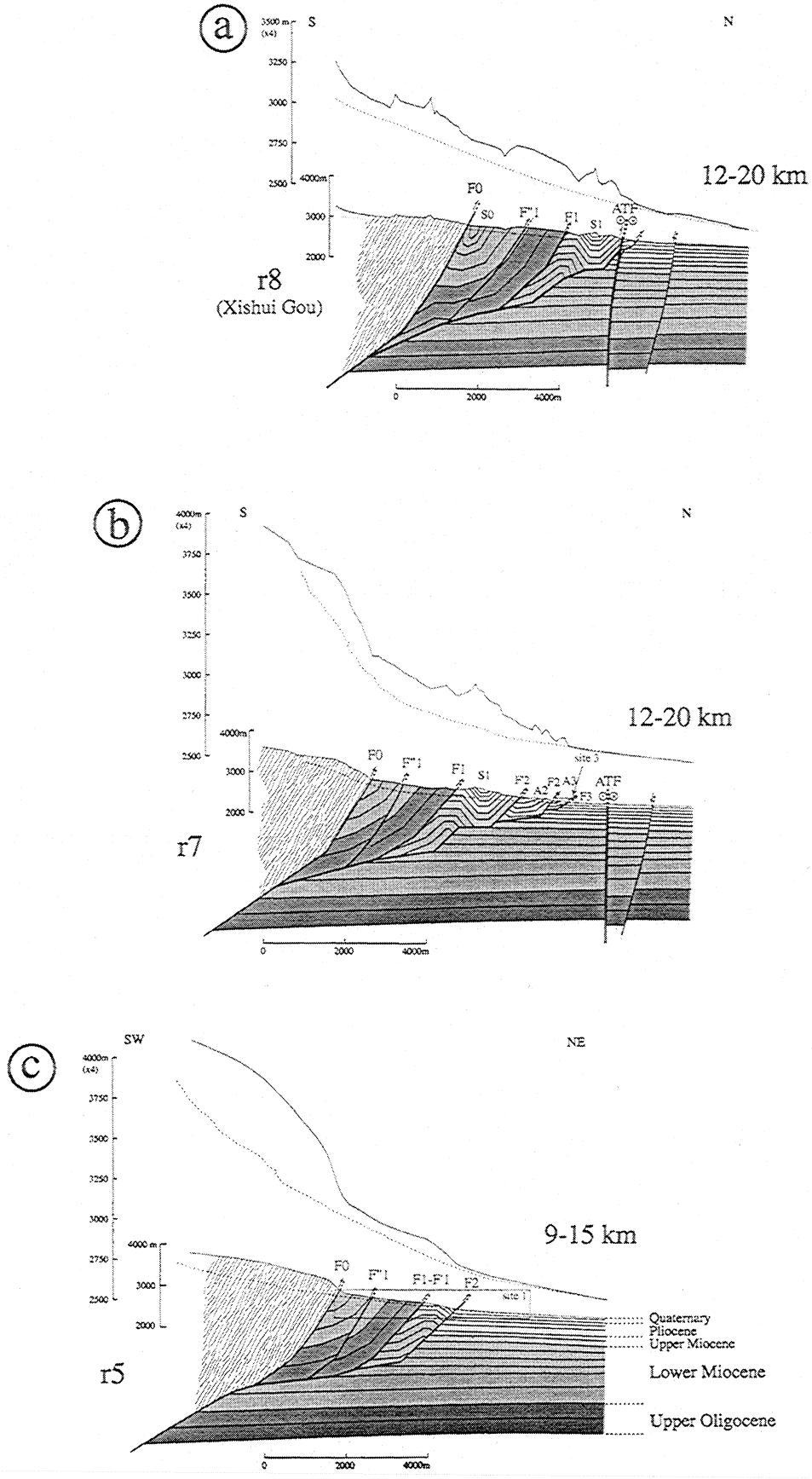

Figure 7. Plausible retrodeformable cross sections across thrust wedge, accounting for field observations (a) along stream r8 (Xishui Gou), (b) along r7, and (c) along r5. Cumulative shortening deduced from balancing of sections is indicated. Topographic profiles of streams and adjacent relief are shown with vertical exaggeration of 4.

gration of thrusting. The asymmetric anticlines formed as fault propagation folds, above steep thrusts ramping to the surface [e.g., *Suppe*, 1983; *Meyer et al.*, 1998]. That anticline (A3), north of F2, exposes only conglomerates, is 200 m wide, and implies that it folds only the shallowest part of the sediment pile and that the thrust beneath it flattens at the base of those conglomerates. The steep thrust ramps to the south have stacked the southern limbs of more evolved, asymmetric anticlines, cutting off most of the recumbent northern limbs [*Yeats*, 1986; *Avouac et al.*, 1993]. The three pinched, asymmetric synclines left stand above hanging wall hinges. The folds and thrusts probably migrated northward as the amount of shortening increased. As along other active range fronts in western China, the thrusts likely root into a master ramp under the range itself [e.g., *Avouac et al.*, 1993; *Gaudemer et al.*, 1995; *Meyer et al.*, 1998]. The exposed thickness of the red beds reaches ~3000 m. Fossils found by *Bohlin* [1937] in the Yadantu valley, 6 km west of Xishui Gou, have upper Oligocene to lower Miocene ages (see also *Regional Geology of Gansu Province* [1989]). The most detailed magnetostratigraphic data along Xishui Gou (r8) between F0 and F1 are more consistent with global chrons between 26 and 19 Ma [*Gilder et al.*, this issue] than with older ages [*Rumelhart et al.*, 1999]. The deep purple red beds and conglomerates between F0 and F1 thus probably straddle the Oligocene-Miocene transition. The lighter red orange mudstones and conglomerates between F3 and F1 are likely of middle to upper Miocene age, and the S1 conglomerates, of uppermost Miocene age. The red beds are conformably folded, in general, although deformation increases toward the range front thrust (F0), reflecting greater burial depth. The growth of the imbricate thrust stack thus probably started in the Pliocene, in agreement with regional stratigraphic constraints [e.g., *Meyer et al.*, 1998; *Métivier et al.*, 1998, and references therein]. The synthetic, retrodeformable sections in Figure 7 (Figure 7a, near Xishui Gou (r8); Figure 7b, near r7; and Figure 7c, along r5 (Plate 1)) based on all the presently available evidence, imply minimum amounts of shortening of ~12 and ~9 km, in ~5 Ma or less.

At the foot of the range, on sections r8 and r7, we saw little or no evidence for present-day movement on F0. On section r8, slip stopped prior to deposition of T3. Terraces along r5 extend across F0 with little disruption (Plate 1 and Figures 8 and 9). At present, only minor slip thus reaches the surface on F0, most of it being transferred at depth on thrusts to the north. T3, which caps much of the F0-F1-F2 ledge, shows comparably minor disruption across the thrusts that separate the red bed slices (F′0, F1, F′1, F′2), consistent with northward migration of thrusting and with the observation that the frontal thrusts (F1, F2, F3) now absorb most of the shortening north of the range.

The strike change, from N100° to N135°E, between F0 and F3, suggests counterclockwise (CCW) rotation of the thrust slices as the thrusts migrated northeastward, in agreement with the paleomagnetic data of *Gilder et al.* [this issue], which attest to -19° ± 5° of CCW rotation relative to the lower Miocene north [*Besse and Courtillot*, 1991].

The steep topographic step that marks the emergence of F2 results from flexural folding of T3. Such folding most likely results from the accumulation of seismic slip increments on F2 at depth even though seismic surface breaks at the base of the step are discontinuous. The earthquake scarplets found on section r7 and north of A3 (Figure 6b) imply that although the entire piedmont thrust must be active, it is probably segmented into short strands with different recurrence times.

2.3. Quantitative Measurements of Terrace Uplift and Folding Along Piedmont Thrusts (F2, F3)

In order to determine recent uplift and shortening rates, topographic leveling was performed across the cumulative, flexural scarp associated with the principal piedmont thrust at three sites. The profiles were measured transverse to the thrust using a digital-recording theodolite-distancemeter (Wild T2000, DI3000). The leveling procedures and related uncertainties are discussed by *Peltzer et al.* [1988], *Avouac et al.* [1993], and *Gaudemer et al.* [1995]. The intrinsic precision of the total station used and the length of the profiles (<5 km) ensures that instrumental errors are a few centimeters at most. Consequently, the roughness of the alluvial surfaces is the main source of error. For the youngest surfaces, the mean size of cobbles on top (diameter of <25 cm) is the primary vertical uncertainty. For older surfaces, smoothing by soil makes irregularities smaller than 20 cm. For the oldest terraces covered by a few meters of loess, the surface smoothness is disrupted by erosion or vegetation. Since depths to the conglomerate layer were not measured, errors on terrace heights are of the order of the erodible loess layer thickness (≤3 m). Such an uncertainty remains small in comparison with the uplift, typically several tens of meters, of the oldest terraces. At each site, the ages of certain terraces south of the main thrust were obtained from ^{14}C dating of organic material dug out of pits or trenches.

2.3.1. Site 1. Site 1 is located where stream r5 cuts F2, about midway along the ledge (Plate 1 and Figures 3b, 8, and 9). As most of the streams that cross the frontal thrust, r5 has deeply incised the highest terrace level (T3). T3 is a meters-thick conglomerate layer, unconformable on 20°-50° south dipping red beds and topped by 1 to 2 m of loess. Further entrenchment of r5 has left two principal inset terraces below T3 (T2, T1; Figures 3 and 8). The minimum height of T3 above the present-day streambed (T0, profile p1, Figure 9) is 47 ± 3 m, and its highest reach, just south of the frontal flexural scarp (F2), is 59 ± 3 m (profile p2, Figure 9, Table 1). T2 is reduced to isolated tongues separated by T1 channels. The two northernmost tongues form

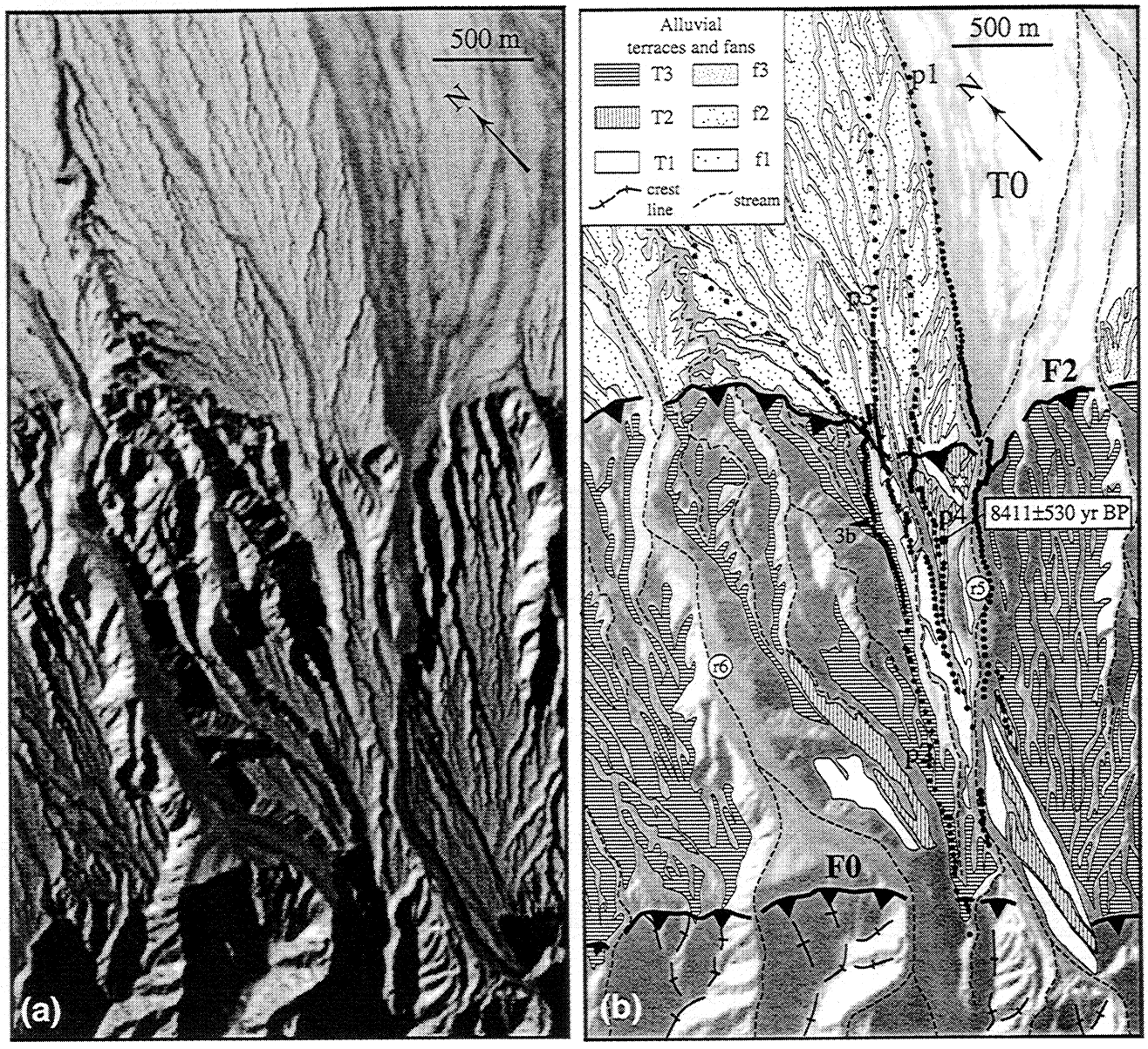

Figure 8. (a) Site 1. Enlargement of SPOT image KJ236-271. (b) Geomorphic interpretation of image in Figure 8a. Solid dots indicate topographic levelling points along profiles p1 to p4 across terrace levels T1, T2, T3 and stream r5.

elongated, teardrop-shaped hills just south of F2, which truncates them at their widest (Figures 3a and 8), a pattern characteristic of progressive folding of terraces across active drainages [e.g., *Meyer*, 1991; *Meyer et al.*, 1998]. The minimum height of T2 above T0 is 26 ± 2 m, and its highest reach, 41 ± 2 m, again just south of F2 (profile p4, Figures 8 and 9). T1 forms a longer tongue, 18 ± 1 m to 24 ± 1 m above T0 (profile p3, Figures 8 and 9). It is also highest immediately south of F2.

Projection of the profiles on a vertical plane striking N45°E, perpendicular to F2 (Figure 9), indicates that T1, T2, and T3 are fairly uniformly uplifted between F0 and F2. At a more detailed level, the three profiles are deformed by a slight synclinal sag whose hinge lies about midway between F0 and F2 and by an asymmetric, north-vergent anticline whose hinge lies ~200 m south of the trace of F2. The terraces thus outline a 1200- to 1400-m-wide bulge south of the main piedmont thrust. The shapes of their warped surfaces may be used to infer the geometry of the underlying thrust ramp. The nonuniform uplift pattern implies a northward increase in thrust dip. More specifically, F2 probably shallows about 1.3 km south of the cumulative scarp, at a depth also of the order of 1.3 km (Figure 7) [e.g., *Meyer et al.*, 1998].

A better assessment of the uplift requires constraints on incision by r5. The downstream decrease in slope (from 6.6° to 6.1°) of the stream profile, which is regularly concave upward, and the steeper slope of T3, which decreases from 8.3° to 6.9° north of F0, may

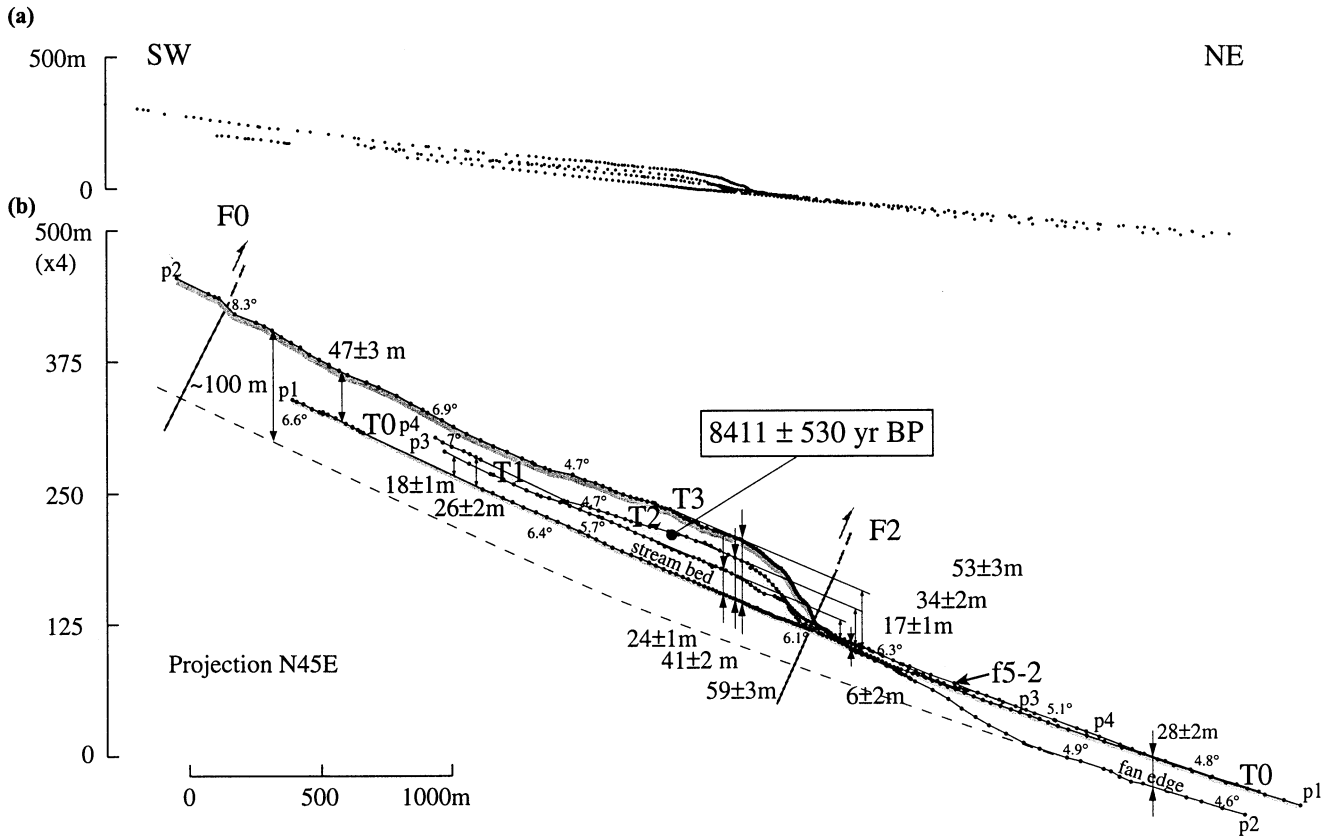

Figure 9. Projection N45°E of profiles at site 1: (a) 1×1 scale; (b) projection with vertical exaggeration (×4). Slopes and heights of terraces above streambed and footwall are indicated. Plausible total offset of T3 inferred from fan slope variation in piedmont may reach ~100 m (see text).

be taken to suggest that the stream gradient changed throughout deposition and folding of the terraces (Figure 9). Although slope differences between the terrace and the river are small (0.5° to 1.7°), a 1° slope variation across a 3000-m-long profile would suffice to account for ~50 m of differential incision. Even if r5 had a steeper slope at the time T3 was deposited, however, the maximum height of the folded terraces relative to footwall bajada profiles north of F2 would not change much. Furthermore, r5 keeps depositing alluvium in its footwall fan, burying the T3 fanglomerates, which leads to an underestimate, probably by 40% (Figure 9), of the actual vertical offset of T3 by F2. The height difference between the streambed profile (p1) and the projection of the distal part of the profile levelled at the western edge of the footwall fan (p2) (Figure 9), where they have similar slopes, reaches 30 m. The thickness of the footwall fan deposited by r5 on top of T3 might be comparable. In any event, relative to the top surface of present deposits on the footwall just north of F2, the minimum vertical offsets of the three terraces (T3, T2, and T1) by the piedmont thrust are 53 ± 3 m, 34 ± 2 m, and 17 ± 1 m, respectively (Figure 9 and Table 1).

Carbon 14 ages were obtained from organic material retrieved by refreshing a steep face cut by a small regressive gully, at the base of the loess mantling the highest reach of T2 (Figure 8 and profile p4 in Figure 9). A bed of angular, poorly sorted clasts of mostly dark green metamorphic Paleozoic schist lies at a depth of 1.3 m under the rather homogeneous loess layer. Just above this uppermost, fluvial T2 deposit, we collected small pieces of black-brown organic matter mixed with loess, probably associated with soil formation after the terrace was abandoned by the river. Three samples weighing less than 1 mg yielded ages of 8330 ± 220, 8395 ± 75, and 9485 ± 485 years B.P. (top in Table 2). The ratio between the minimum throw of T2 across F2 (34 ± 2 m) and the weighted mean of these three ages (8411 ± 530 years B.P., top in Table 2) provides a minimum vertical uplift rate of 4.1 ± 0.5 mm/yr for this terrace during the later part of the Holocene. If this rate had remained constant between the Last Glacial Maximum (LGM)(~20 ka) and the present, the ages of T3 and T1 would be 14390 ± 3200 years B.P. and 5850 ± 1000 years B.P., respectively. If the dip of the main piedmont thrust ramp F2 were less than 45°S, then the shortening rate across the north flank of the Tanghe Nan Shan range would significantly exceed 4 mm/yr.

2.3.2. Site 2. Site 2 is located where the surface traces of thrusts F2 and F3 meet the most active strike-slip strand of the Altyn Tagh Fault (Plate 1 and Figure 10). The thrusts have produced uplift and folding of

Table 1. Heights of Terraces Above Streambeds and Vertical Throws Across Main Thrusts

Terrace	Profile	Height, m	Vertical Throw, m		Seismic Scarp Height, m
			F2	F3	
Site 1					
T1	p3	24 ± 1	17 ± 1	...	
T2	p5	41 ± 2	34 ± 2	...	
T3	p2	59 ± 3	53 ± 3	...	
Site 2					
T0	p4	1.1	...	...	
T0	p4	4.5	...	...	
T1	p4	13.3	...	...	
T′2	p4	31.0	...	...	
T″2	p4	36.2	...	...	
T‴2	p7	...	...	3 ± 1	
T″3	p4	45.4	...	...	
T‴3	p4	47.9	...	...	
T‴3	p10	...	15 ± 3	...	
T‴3	p9	...	14 ± 3	11 ± 3	
Site 3					
T0	p9	1.3	...	...	...
T1	p10	...	...	2.3	0.9
T1	p5	4.5	...	3.3	1.6
T1	p13	...	...	2.6	1.4
T1	p12	...	...	...	1.6
			mean	3.0 ± 0.3	1.5 ± 0.1
T′1	p3	...	...	4.2	0.7 - 1.9
T′1	p2	...	...	4.6	1.5 - 2.9
T′1	p1	...	...	4.5	1.1 - 2.1
			mean	4.5 ± 0.5	
T2	p3	...	...	14.8	
T2	p8	18.1	...	14.6	
			mean	14.7 ± 0.1	
T′2	p7	...	...	22.4	
T′2	p2	...	...	17.1	

now abandoned terraces north of the present channel of Xishui Gou (r8) (Figure 10). North of the thrusts, the Altyn Tagh Fault is marked by a continuous, north facing scarp across recent fans (Figure 10).

The terraces and fans form a set of hanging, inset tongues of fluvial alluvium, which could only have been emplaced by the Xishui Gou stream before its course was deviated eastward into its present channel (Plate 1 and Figures 2 and 10). The fans are left laterally offset several tens to hundreds of meters by the fault [*Van der Woerd*, 1998]. Four main terrace levels (T1 to T4), each divided into sublevels, form a total of 10 distinct surfaces. All are conglomeratic strath terraces cut into the steeply dipping, Oligocene-Miocene red beds as at site 1. Almost all the terraces are covered with a loess layer whose thickness increases with height above the present streambed, attesting to successive abandonment during incision, and final entrenchment of r8 into its present channel. The inset arrangement of the terraces and the pattern of smaller rills on their surfaces confirm that they were deposited by a fairly large, more northerly flowing stream (N2°E to N30°E, Figure 10). Such a flow direction is that of r8 upstream, before it bends sharply eastward just south of the site. The now beheaded and hanging terraces, deposited by r8, were thus probably abandoned while the stream incised deeper toward the east, as a consequence of capture by a smaller stream whose headward retreat was driven by thrusting and folding. The more recent levels (T′0, T1, Figure 11) were emplaced along the N70°E trending present channel, after r8 abandoned T″2, the last north directed outlet before capture.

Table 3. Model Age of Terraces at Site 2

Terrace	Height Above Stream, m	Model Age, years
T0	1.1 ± 0.2	380 ± 50
T′0	4.5 ± 0.2	1150 ± 230
T1	13.3 ± 0.5	4582 ± 143[a]
T′2	31.0 ± 2.0	7442 ± 340
T″2	36.2 ± 2.0	9235 ± 130[a]
T″3	45.4 ± 2.5	12400 ± 540
T‴3	47.9 ± 2.5	13270 ± 400

[a]Terrace directly dated with radiocarbon.

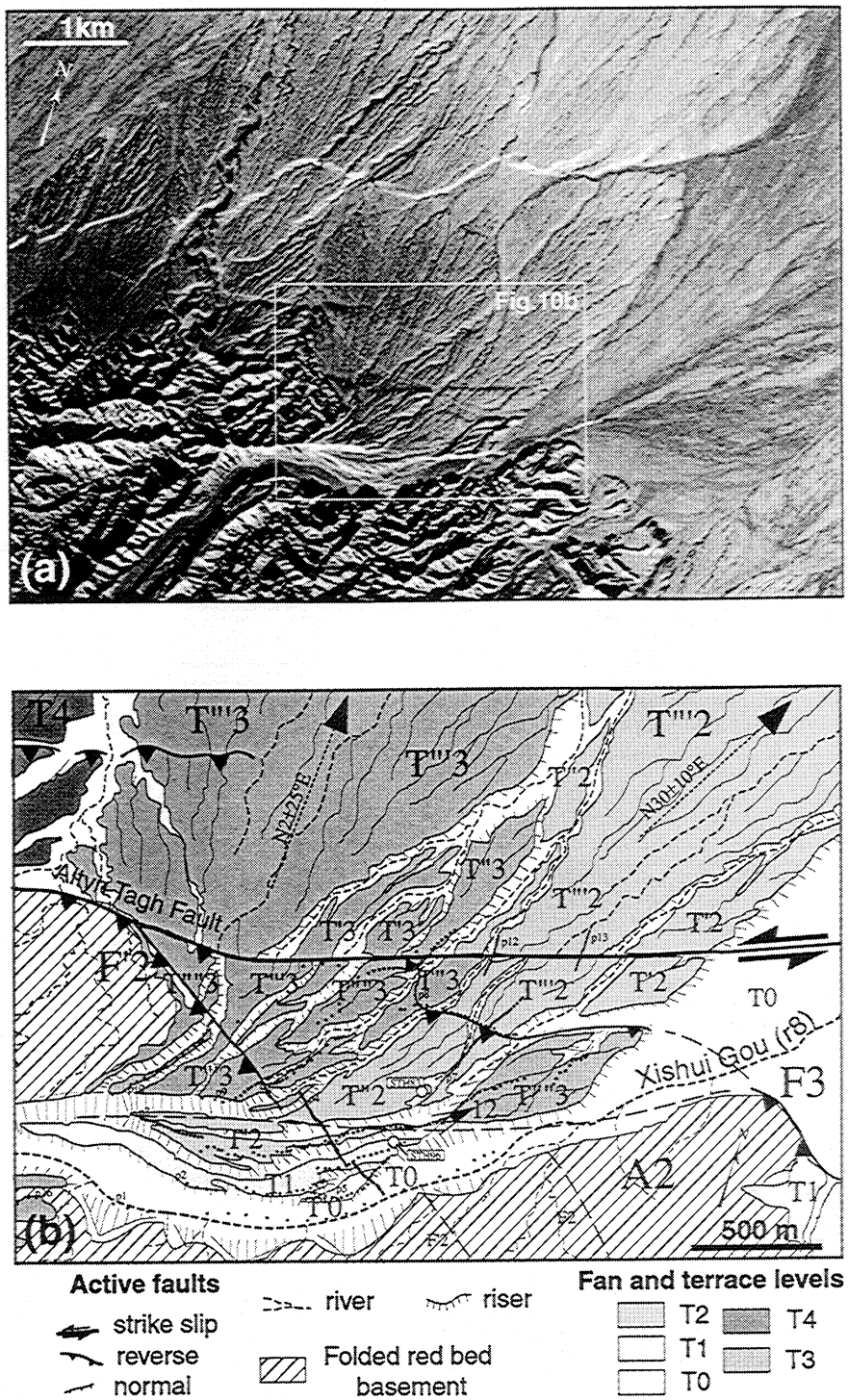

Figure 10. (a) Enlargement of SPOT image KJ236-271 of site 2. (b) Geomorphic interpretation of white rectangle in Figure 10a. Solid dots are topographic profile points. Large white dots are sampling sites for radiocarbon dating. Terrace chronology and slope directions suggest deviation of stream r8 from N to NE (T3 to T2) and then capture into present-day channel (from NE to approximately E-W).

Total station profile p4 (Figure 11) shows the heights of the principal terraces above the present-day streambed (Table 1). The ages (4582 ± 172 years B.P. and 9235 ± 130 years B.P.; Table 3) of two of the terraces (T1 and T″2, respectively) were determined by ^{14}C dating of charcoal and organic material sampled just above the limit between pebbles and overlying loess in pits and trenches dug on top of the terrace surfaces (Table 2). The ratios between the height above the present-day streambed and the age of these two terraces (2.9 ± 0.2 mm/yr and 4.9 ± 0.2 mm/yr for T1 and T″2, respectively) reflect a marked difference in incision rate. This

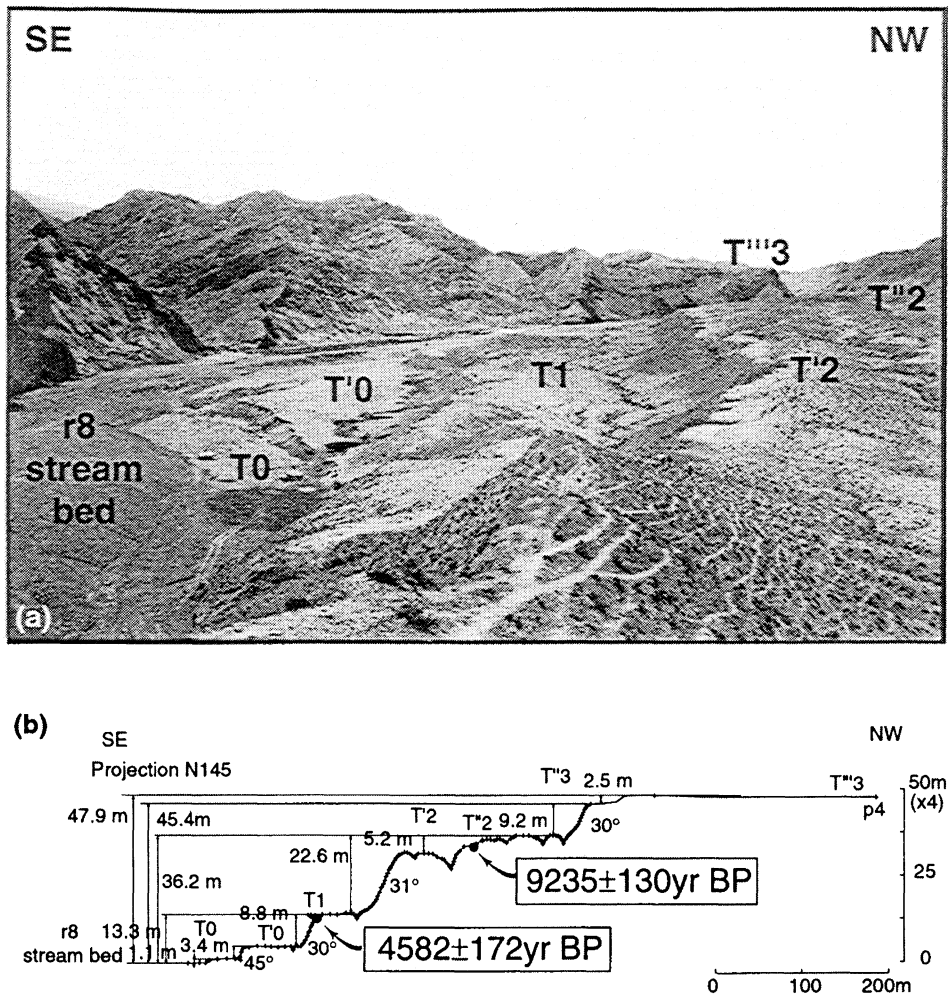

Figure 11. (a) View, to the west, at site 2, of abandoned terrace flight above entrenched streambed r8. (b) Profile p4 across terraces and relative heights.

suggests that capture occurred between the emplacement of T′2 and T1, as implied by the great height (17.4 m) of the T″1/T1 riser (Figure 11), with a mean incision rate prior to capture comparable to that since abandonment of T1 (Figure 12). Capture would have instantaneously lowered the base level of the stream, increasing greatly, but briefly, the incision rate, possibly around 5500 years B.P.. Following this scenario, and despite the uncertainty in the timing of capture, it is possible to infer the ages of the other terraces (Table 3), which would range from 380±50 years for T0, 1550±230 years for T′0, 7440 ± 340 years for T′2, 12,400 ± 540 years for T″3, and 13,270 ± 400 years for T‴3 (Figure 12).

From profiles p10 and p9, the vertical throw of T‴3 appears to be about 14 ± 3 m across F′2 and about 11 ± 3 m across F3 (Figure 13). The latter throw may be overestimated, since it includes the apparent vertical offset due to left-lateral displacement of the sloping terrace surface by the Altyn Tagh Fault [*Van der Woerd*, 1998]. The difference between the highest level reached by T‴3 south of r8 and the level of the T‴2 fan north of both thrusts implies that the minimum cumulative vertical throw probably exceeds ~50 m, an offset comparable to that of T3 at site 1 (53±3 m). Note, however, that the strikes of F′2 and F3 are about N120°E and N85°E, 15° and 50° less, respectively, than the strike of F2 at site 1 (N135°E). Such differences in strike might account for variations in coeval shortening, hence uplift amounts of 5% to 50%, such that the vertical throw of T‴3 might be roughly half that at site 1 consistent with the sum of the vertical throws of T‴3 across both F3 and F′2 along profile p9 (25 ± 6 m, Figure 13). The vertical throw of T2 across F′2 cannot be measured because entrenchment of r8 has destroyed the intersection between F′2 and T2. The total throw of terrace T2 is thus poorly constrained. Nevertheless, overall, both the ages of the terraces and the measured throws indicate a pattern of cumulative uplift quantitatively comparable with that at site 1.

2.3.3. Site 3. At this site, about halfway between the present outlets of r7 and r8 onto the bajada (Figure 2), five hills capped by folded fanglomerates mark the growth of a 1250-m-long and 200-m-wide anticline (A3,

Table 2. Radiocarbon Dating Results at Sites 1, 2, and 3

Sample	Fraction Modern, 10^{-2}	$\Delta^{14}C$	Radiocarbon Age[a], years	Calibrated Age[b], years B.P.	Sample Depth, cm
Site 1					
Terrace T2					
STH48c	39.01 ± 1.12	...	7500 ± 240	8330 ± 220	1.3
STH48d	36.05 ± 0.31	-639.5 ± 3.1	8200 ± 80	9485 ± 485	1.3
STH48e	38.54 ± 0.44	-614.6 ± 4.4	7660 ± 100	8395 ± 75	1.3
			mean:	8411 ± 530	
Site 2					
Terrace T1					
STH96a	58.86 ± 0.33	-401.4 ± 3.3	4120 ± 50	4635 ± 185	0.3
STH96b	60.99 ± 0.39	-390.2 ± 3.9	3970 ± 60	4410 ± 60	0.3
STH96c	58.97 ± 0.46	-410.3 ± 4.6	4240 ± 70	4725 ± 35	0.2
STH96d	60.01 ± 0.39	-399.9 ± 3.9	4100 ± 60	4470 ± 40	0.1
			mean:	4582 ±1 72	
Terrace T″2					
STH83a	43.82 ± 0.37	-561.8 ± 3.7	6630 ± 70	7505 ± 25	~1
STH83b	36.15 ± 0.21	-638.5 ± 2.1	8170 ± 50	9105 ± 105	~2
STH83c	35.59 ± 0.23	-644.1 ± 2.3	8300 ± 60	9280 ± 90	~2
STH83d	36.21 ± 0.21	-637.9 ± 2.1	8160 ± 50	9305 ± 105	~2
			mean:	9235 ± 130	
Site 3					
Terrace T′0					
STH61a	90.94 ± 0.69	-90.6 ± 6.9	760 ± 70	690 ± 30	0.4
STH61b	91.34 ± 0.51	-86.6 ± 5.1	730 ± 50	670 ± 20	0.4
STH62a	97.72 ± 0.65	-22.8 ± 6.5	180 ± 60	145 ± 72	...
STH62b	91.67 ± 0.89	-83.3 ± 8.9	700 ± 80	625 ± 65	...
Terrace T1					
STH64	83.45 ± 0.45	-165.5 ± 4.5	1450 ± 50	1340 ± 40	0.43
STH67a	98.59 ± 0.65	-14.1 ± 6.5	110 ± 60	135 ± 67	0.1
STH67b	90.94 ± 1.04	-90.6 ± 10.4	760 ± 100	690 ± 40	0.1
STH67c	91.10 ± 1.82	-89.0 ± 18.2	750 ± 170	715 ± 165	0.1
STH67d	86.57 ± 0.58	-134.3 ± 5.8	1160 ± 60	1070 ± 100	0.2
STH67f	86.92 ± 2.07	...	1130 ± 200	1025 ± 245	0.3
STH67h	80.00 ± 1.36	...	1790 ± 140	1615 ± 95	0.2
Terrace T2					
STH67g	36.11 ± 0.25	-638.9 ± 2.5	8180 ± 60	9100 ± 110	1.0

[a]Radiocarbon age using the Libby half-life of 5588 years, an assumed $\delta^{13}C$ value of -25, and following the conventions of *Stuiver and Polach* [1977].

[b]Calibration according to *Stuiver and Reimer* [1993]. Mean value between lower and upper bound.

Figure 14). The main stream that drains the catchment between r7 and r8 has abraded the central part of the anticline, depositing a younger set of terraces now folded and uplifted at different heights above the streambed. West of the easternmost stream channels, the uplifted terraces are bounded to the north by one or two recent seismic thrust scarps. East of that channel, a slope break marks the base of a large flexure (Figure 14). The highest terrace levels here (T2 and T′2) stand 14.6 and 22.4 m, respectively, above the fan north of the slope break (profiles p8 and p7, Figure 15). West of the main stream, two elongated terrace tongues, the highest one with a narrow, eroded crestline perpendicular to the fold axis, stand 14.8 and 17.1 m above the fans north of the thrust scarps (p2 and p3, Figure 16). These terrace tongues thus correlate with the levels on the east side of the stream (Figure 14). They are surrounded by a lower level (T′1) only 4.5 m above the northern fans (p1, p2, and p3, Figure 16). An even lower terrace level, T1, forms an isolated tongue between the two principal channels of the stream, 2.3 to 3.3 m above the same level north of the thrust scarp (p13, p5, and p10, Figure 15). The lowest terrace level (T′0), last abandoned by the stream, stands only 1.3 m above the streambed. It is paved with loose surface pebbles thinly sprinkled with loess and bears well-preserved braided channels (Figure 17). T1 has a smoother surface, with a 0.3- to 0.5-m-thick loess cover, but is still bounded by sharp and steep risers (Figure 17). T′1, T2, and T′2 have loess covers of increasing thickness (from 1 to 2 m) and risers eroded by deep, regressive gullies.

Charcoal samples (STH61a and STH61b; 1, in Figure 14) were retrieved in T′0 near the top of a free faced riser, ~70 cm above the streambed and ~40 cm beneath the surface (Figure 17). Such charcoal, apparently from a camp-fire, was found clustered within a ~2-cm-thick,

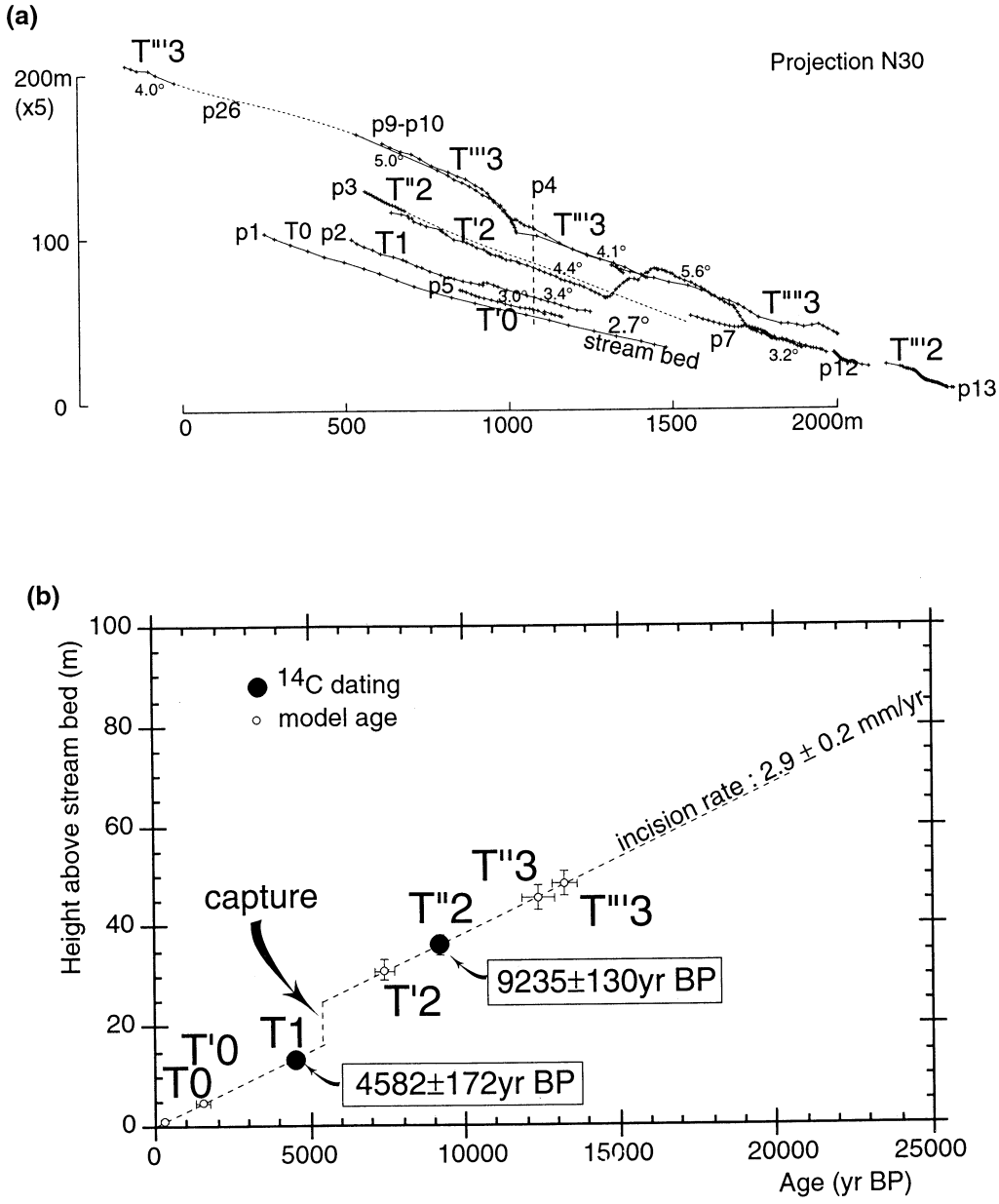

Figure 12. (a) Topographic profiles projected N30°E at site 2. (b) Age of terraces, inferred from incision rate assumed to be constant and two dated terraces (T1 and T″2).

~2-m-long sand lens in between gravel layers. Two fragments yielded similar ages of 690 ± 30 years B.P. and 670 ± 20 years B.P. (Table 2). Two other samples were found near the top of another riser upstream (2, Figure 14). Small roots just under the surface (STH62a) and a deeper charcoal (STH62b) yielded ages of 145±72 years B.P. and 625±65 years B.P., respectively. The surface of T′0 is thus younger than 650 years B.P., in agreement with its modest height (~1 m) above the present-day streambed and the braided channels still visible on it. The thin loess layer and vegetation, however, suggest it was abandoned centuries ago.

On T1, samples were collected in two different places. On the east bank of the western channel (4, Figure 14), a free-faced riser exposes ponded T1 deposits with intercalated gravel, sand, and reworked loess layers down to about 1 m upstream from a protruding T2 remnant (Figure 18). Samples STH67a-STH67f were collected near the top of the section, down to 0.3 m. The topmost samples are charcoal from small bush trunks probably resulting, like STH62a, from vegetation burial by loess accumulation and soil on the surface of the abandoned terrace. From deepest to shallowest, their ages (STH67a, STH67b, STH67c) range between 715 ± 165 years B.P. and 135 ± 67 years B.P., corroborating upward younging of the soils (Figure 18). Gravel beds underneath become coarser downward and alternate with sandy layers. The three samples just beneath the

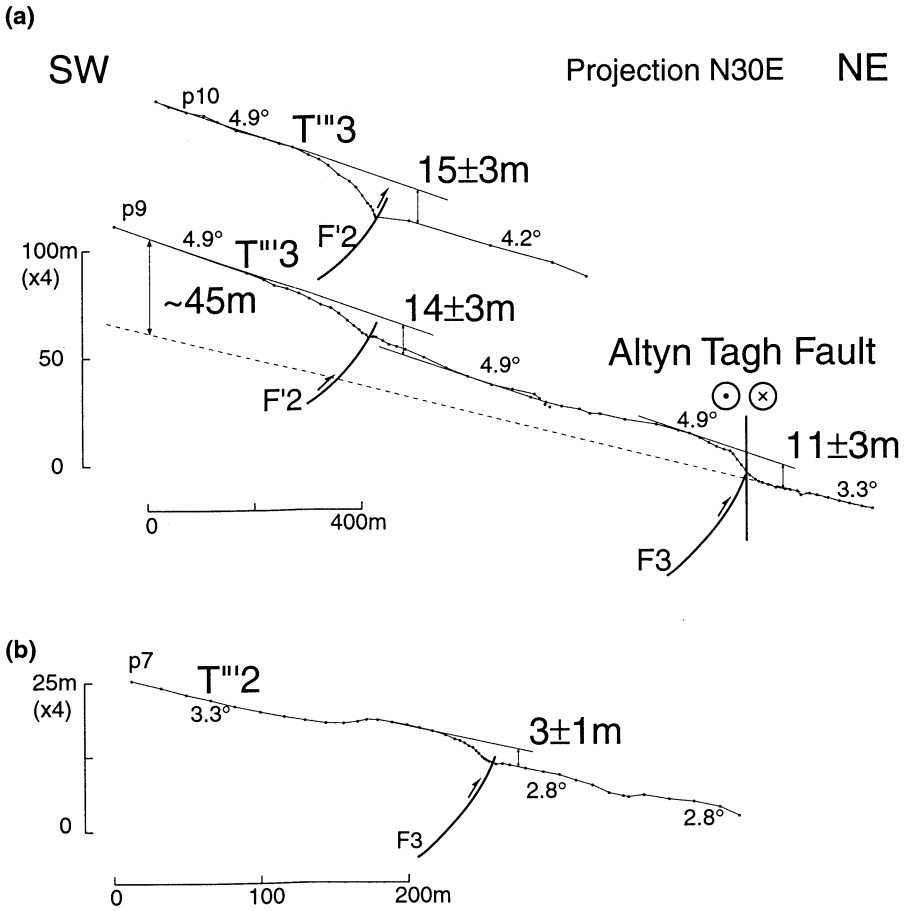

Figure 13. (a) Projection N30°E of profiles p10 and p9 across F2 and F3 and vertical throw across different thrusts. (b) Profile p7 across F3 on T'''2.

shallowest pebble and gravel beds (STH67d, STH67f, STH67h) have older ages of 1070 ± 100, 1025 ± 245, and 1615 ± 95 years B.P., which constrain the last episodes of fluvial deposition on T1. The age of abandonment of T1 must postdate 1615 ± 95 years B.P.. The deepest sample (STH67g), collected 1 m beneath the surface in a thin sand lens within the coarsest pebble layer, yields an age of 9100 ± 110 years B.P.. This much older sample probably belongs to T2, like the adjacent, protruding coarse conglomerate remnant that locally dams the T1 deposits. T2 is therefore younger than 9100 years B.P.. A trench dug into the loess cover of T1 (3, Figure 14), about 70 m east of the western channel riser (Figure 17), yielded another charcoal sample (STH64), 0.43 m beneath the surface, with a calibrated age of 1340 ± 40 years B.P. (Table 2), consistent with those of STH67d, STH67f, STH67h. This confirms that T1 was abandoned sometime between 1300 and 1000 years B.P..

A minimum vertical throw rate on F3, 1.6 mm/yr (Figure 19), can be calculated using the ratios between the minimum vertical offsets (2.3 and 14.6 m, Table 1) and the maximum ages (1340±40 years B.P. and 9100± 110 years B.P., Table 2) of T1 and T2, respectively. If the vertical offset of T1 had been 3.3 m in as little as 1025 years B.P. (Tables 1 and 2), then the maximum throw rate on F3 would be about 3.2 mm/yr. The best constrained vertical throw rate is that obtained by using the offset of T1 on p5 (3.3 m, Figure 15, Table 1) and the age of T1 in the trench less than 20 m from that profile (1340 years B.P.). It is 2.46 mm/yr, close to the mean between the bounds above (2.4 ± 0.8 mm/yr)(Figure 19). Assuming the thrust ramp beneath anticline A3 to dip 45° would imply a shortening rate of ~2.5 mm/yr across F3 and this anticline.

The well-preserved seismic thrust scarplet (Figure 17) that cuts the T1 terrace tongue between the main stream channels does not extend on T'0. On profiles p13 and p5 (Figure 15a), the height of the scarplet is 1.4 to 1.6 m. On p10 (Figure 15a), it is smaller (0.9 m), because of lateral aggradation at its base. The scarplet slope is still steep (~23°), with no break, and thus the ~1.5-m surface offset results from only one earthquake, predating the emplacement of T'0, probably around 600 years ago. To the west, the scarplet continues 200 m to merge with the higher cumulative seismic scarps that offset T'1 vertically by 4.5 m (Figure 17). The cumulative vertical offsets of T1 on p5 and p13 are about twice

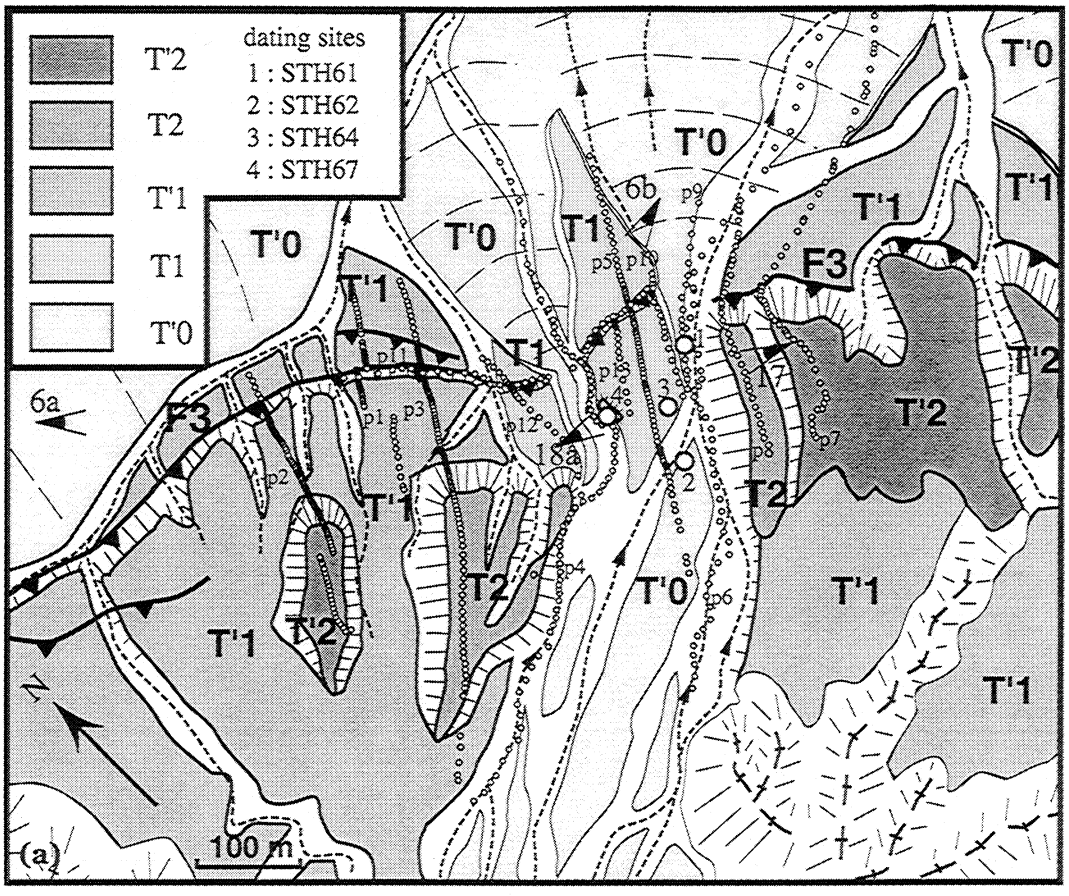

(b)

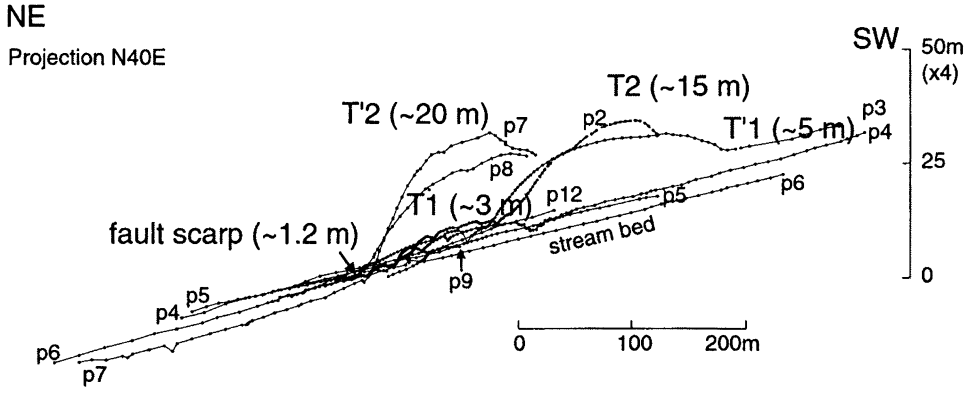

Figure 14. (a) Geomorphic map of site 3. Hills correspond to anticline A3. Note scarps of thrust F3 that bound A3 to the northeast. Small dots are levelling points of topographic profiles. Large dots refer to sampling sites for radiocarbon dating. (b) Projection of topographic profiles across anticline A3 at site 3.

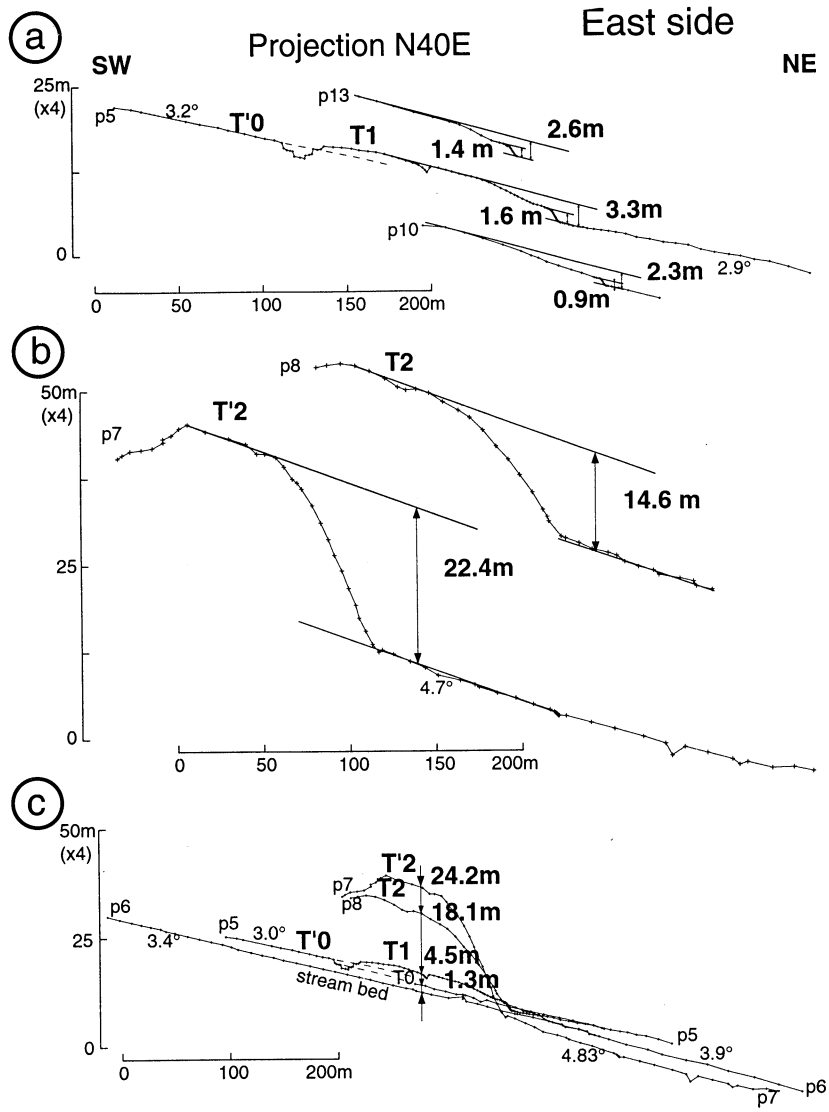

Figure 15. Topographic profiles across anticline A3: (a) on terrace T1 and across scarp F3, (b) on T2 and T′2 east of the stream, and (c) relative heights of terrace levels above the active streambed.

the height of the seismic scarplet (Table 1) and thus appear to result from two similar earthquakes. These two events would have occurred in the last 1000-1300 years, consistent with a recurrence time of the order of 600-700 years (Table 2). The 4.5-m offset of T′1 farther west could be due to three comparable events, each with a throw of ~1.5 m, implying that T′1 is at least 1800-2400 years old.

3. River Incision Along the Western Front of the Tanghe Nan Shan

In order to determine tectonic uplift of an alluvial surface, one must know the geometry of the surface at the time it was deposited [*Weldon*, 1986; *Bull*, 1991; *Meyer et al.*, 1998]. In the simple case where faulting and folding are narrowly localized transverse to a river course, such initial geometry can be derived by extrapolating, across the fold, the undeformed reaches of the surface on either side [*Rockwell et al.*, 1988]. For instance, fault bend or fault propagation folds that grow on top of thrust ramps at the tip of flat décollements that reach far into the piedmont of growing ranges [*Avouac et al.*, 1993; *Meyer et al.*, 1998] are usually cut by graded rivers that can be considered to maintain stable profiles, providing reference levels to measure uplift [*Avouac et al.*, 1993; *Lavé and Avouac*, 2000; *Meyer et al.*, 1998]. At Subei, the proximity of the steep range front and the existence of captures suggest less stable river slopes. However a quantitative assessment of the shapes of river profiles and of the catchments along the range front (Figures 20 and 21) makes it possible to compare incision and tectonic uplift rates.

Absolute dating of the terraces at the foot of the

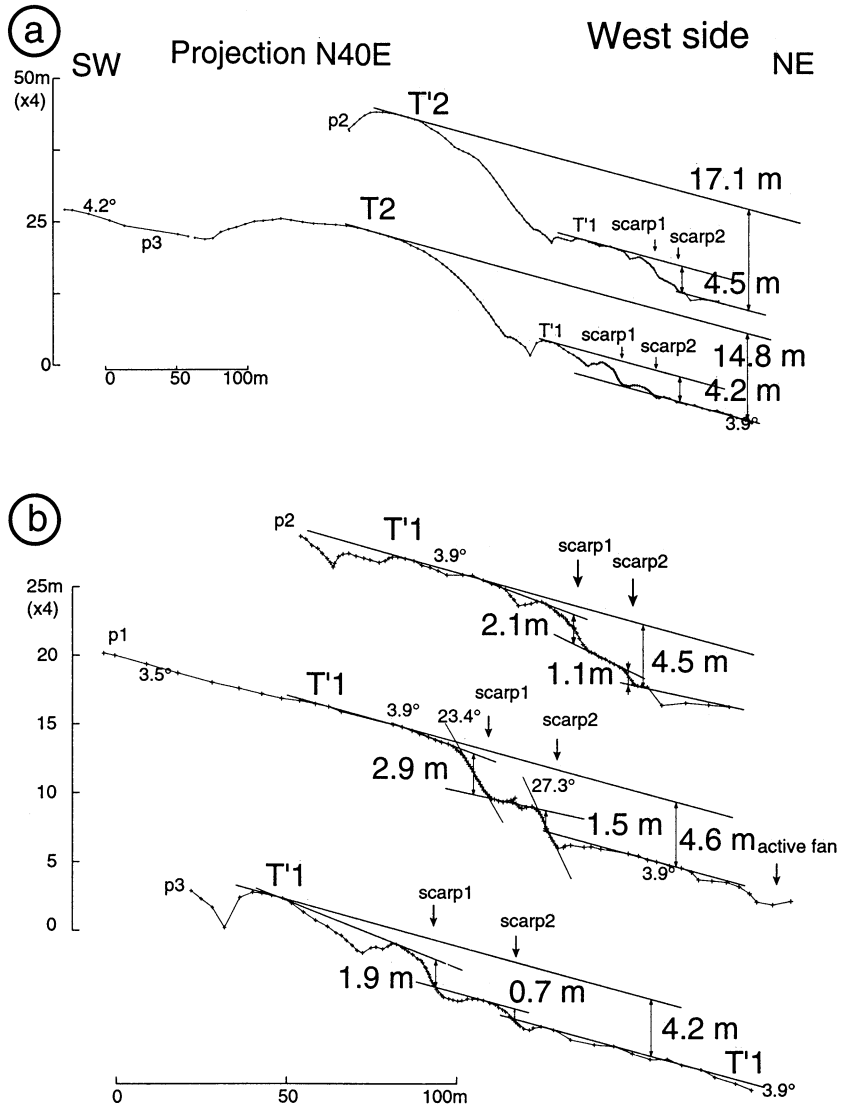

Figure 16. (a) Topographic profiles on T2 west of the stream. (b) Topographic profiles on T′1 and across F3 scarp.

range implies that most postdate the LGM. Such young terraces are thus well preserved and fairly continuous, and the geometry of their folded surfaces, well constrained. Because of their fairly steep slope (>3°) upon a narrow ledge (~3 km), such terraces are probably synchronous treads, and the rate of shortening is likely to have been constant over the short time span since the LGM. The uniform morphology and height of the ledge between r1 and r8 (Plate 1) suggest a uniform tectonic regime along the piedmont, making compari-

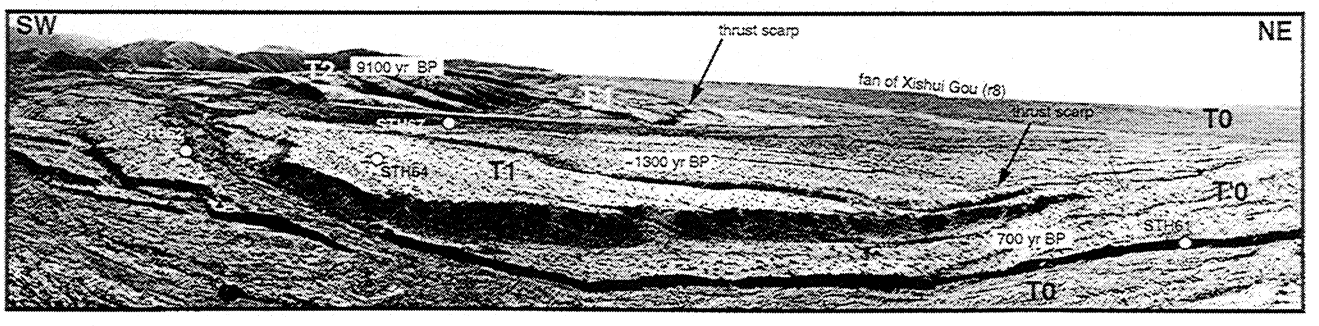

Figure 17. View to the northwest of folded and faulted lower terraces (T′0 and T1) at site 3. Ages of terrace abandonment deduced from radiometric dating are indicated (see text).

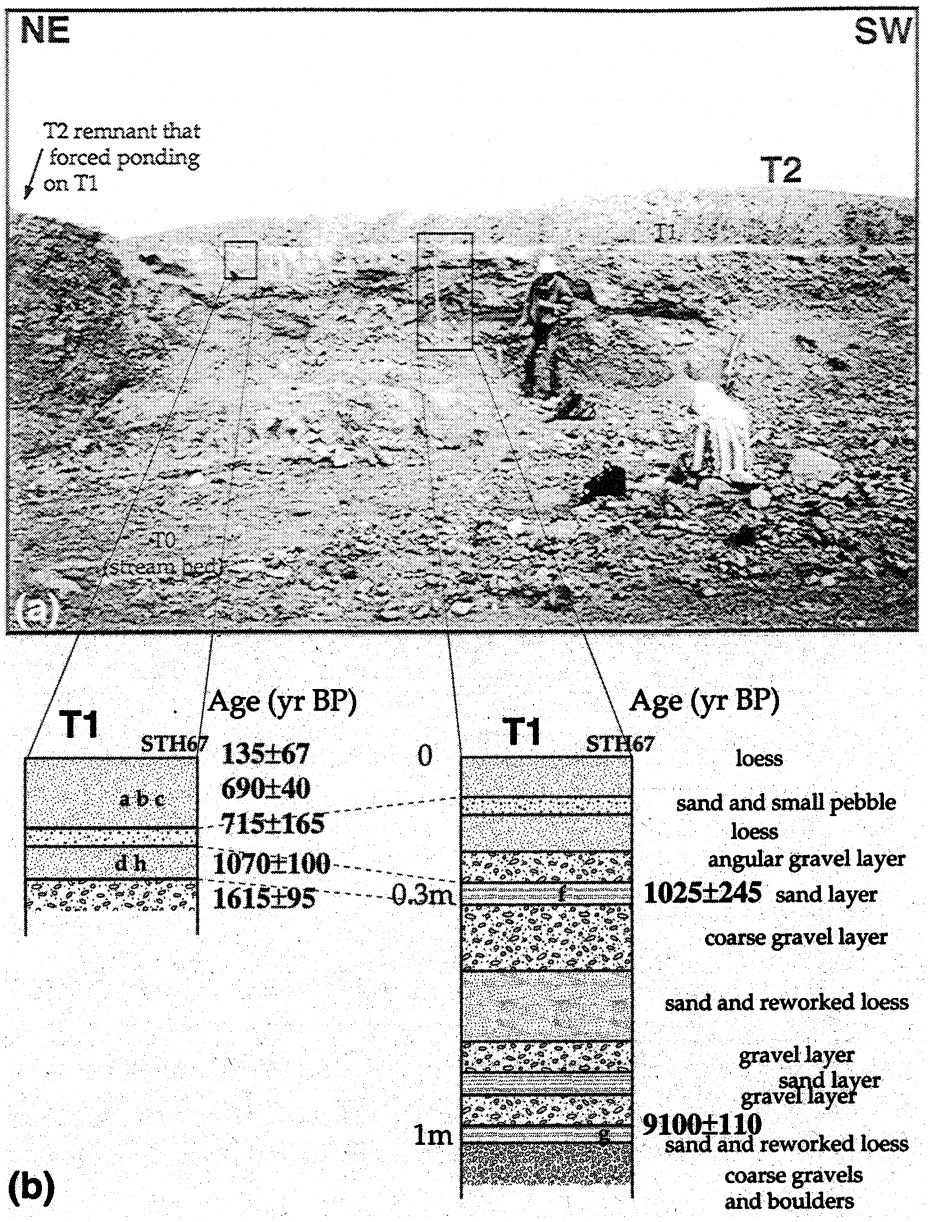

Figure 18. (a) View of refreshed T1 riser. (b) Descriptive logs and charcoal sampling sites (lettering "a" to "h") with ages in years before present.

son between the different streams possible. Except for three streams (r1, r5, and r8), the stream catchments are of comparably small size (Figure 20). Almost all the catchment areas are within the same unit of Paleozoic rocks, except for streams r1 and r8, which have the largest catchments. Finally, regional base level changes in the Subei basin are negligible: the total amount of entrenchment of the Tanghe River in the Subei plain during the last 14,000 years (20-30 m [*Van der Woerd*, 1998]) is too small to have affected the small streams that flow across the thrusts.

Figure 21 shows the profiles of streams r1 to r8 (from the 1:50,000 scale topographic map; contour spacing, 10 m), with profile slopes calculated as means between a minimum of three points. For the longest profiles (r1, r8, and r5), only the northern parts are shown. All three have gentle, more regular slopes. The other stream profiles are markedly different. They show sharply concave upward shapes with a marked slope break near F0. This shape reflects the varying erosional and depositional behavior of the streams in three different domains: the watershed in the rising metamorphic basement, the terrace-capped red bed ledge, and the piedmont bajada. The zone of sharpest curvature lies just downstream from F0, in the upper part of the Oligocene-Miocene thrust wedge. The profile slopes start at 2°-5° in the depositional bajada to reach 5°-8° between F1 and F0, downstream from the slope break. The slopes then increase rapidly to 14° or more. The highest values (30° to 60°) are on the faceted basement spurs. Streams r1,

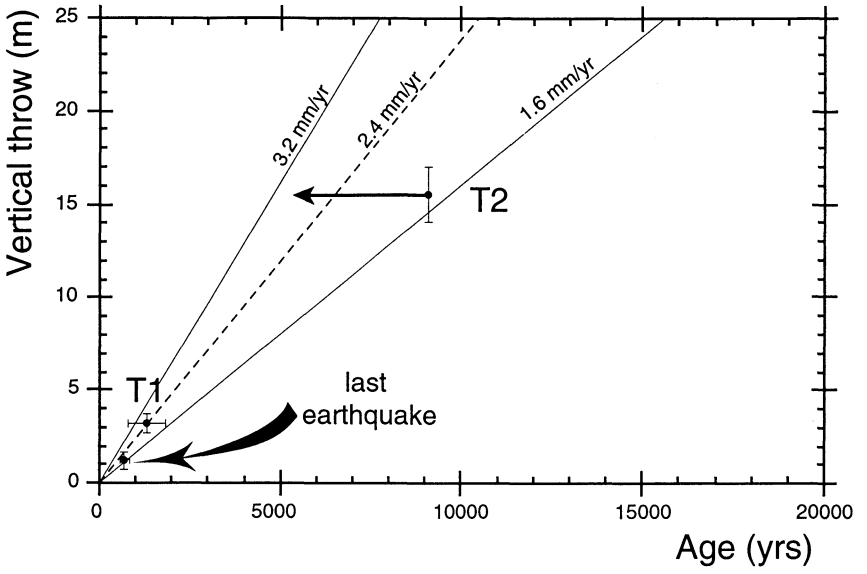

Figure 19. Inferred vertical uplift rate from vertical throw of terraces T2 and T1 at site 3.

r5, and r8 have gentler overall slopes and curvature because the headwaters of their larger catchments lie far beyond the crest of the range (Figure 20). Because fans develop where streams widen as they lose power and start to aggrade, fans generally have slopes similar to that of streambeds upstream from the fan apex [*Bull*, 1991]. This holds here for the most recent fans whose apices lie at the outlet of the intermittent streams onto the bajada (Figure 21), but older fans (f1-f2, Figure 22) have steeper slopes and are reincised by the present-day streams.

Because they cross the thrust ledge in a more distal part of their course, r1, r5, and r8 have an incision-deposition regime different from that of the other streams. The latter cross the ledge immediately after the precipitous upper part of their watersheds on the steep basement facets; hence the prominent slope break observed on their profiles. The difference in incision is clear in Figure 22, where stream, fan, and T3 terrace profiles (r3 to r7) are projected together. Except for r5, all are entrenched 100-130 m into the ledge and maintain a profile that merges smoothly with the distant bajada level upon which they deposit their present fan, while incising 30 to 50 m below the level of their older fans north of F1. By contrast, r5 remains perched 20 to 50 m above the level of the bajada. This is also clear in the longitudinal profiles parallel to the range front (Figure 20c), where the r5 streambed stands atop a depositional swell, ~50 m above the bajada level north of F1. The active fan of r5 is the only one whose apex reaches F1 and stands at the level of its older fan apex, while all other streams incise their fan heads on the footwall of the thrust. Xishui Gou (r8) shows a similar behavior (Figure 20c). In short, r5 and r8 have less incisional power. They cross the thrust ledge in a more aggradational part of their course, while the other streams, whose profiles in the ledge are close to the steepest part of their watershed, can only incise as they cross it and start depositing their debris farther north, well into the bajada.

That the small streams have more incisional power is corroborated by the vigorous headwater retreat observed in their uppermost watersheds. The short streams that flow northeast, perpendicular to the Subei thrust and range front, tend to capture the longer, older streams that flow more gently toward the northwest (Figure 20b). For instance, only a narrow crest, barely ~10 m above the perched bed of the eastern tributary of r8, separates it from the precipitous headwaters of r7, whose profile slope break lies nearly 200 m below (Plate 1 and Figure 20). Capture of the former by the latter is thus imminent. At site 2, ~5000 years ago, a similar event led r8 to abandon its T″2 channel and fan, now beheaded and perched 36 m. This capture triggered rapid incision in the lower part of the stream course, now entrenched ~80 m below T3, south of F′2. Such entrenchment, in turn, brought the streambed of r8 across the northern part of the thrust ledge in continuity with the lower bajada slope.

4. Discussion and Conclusion

Three distinct behaviors are expected for streams crossing active thrusts. A stream may incise more than the rocks move up owing to thrusting and hence incise also its footwall fan where there is no tectonic uplift. Such behavior typifies places where a pluvial causes renewed, vigorous incision or where the base level drops down. Stream incision can keep pace with tectonic uplift. The tectonic uplift rate may exceed the incision power of a stream, in which case its bed becomes perched. Here, along the steep Tanghe Nan range front

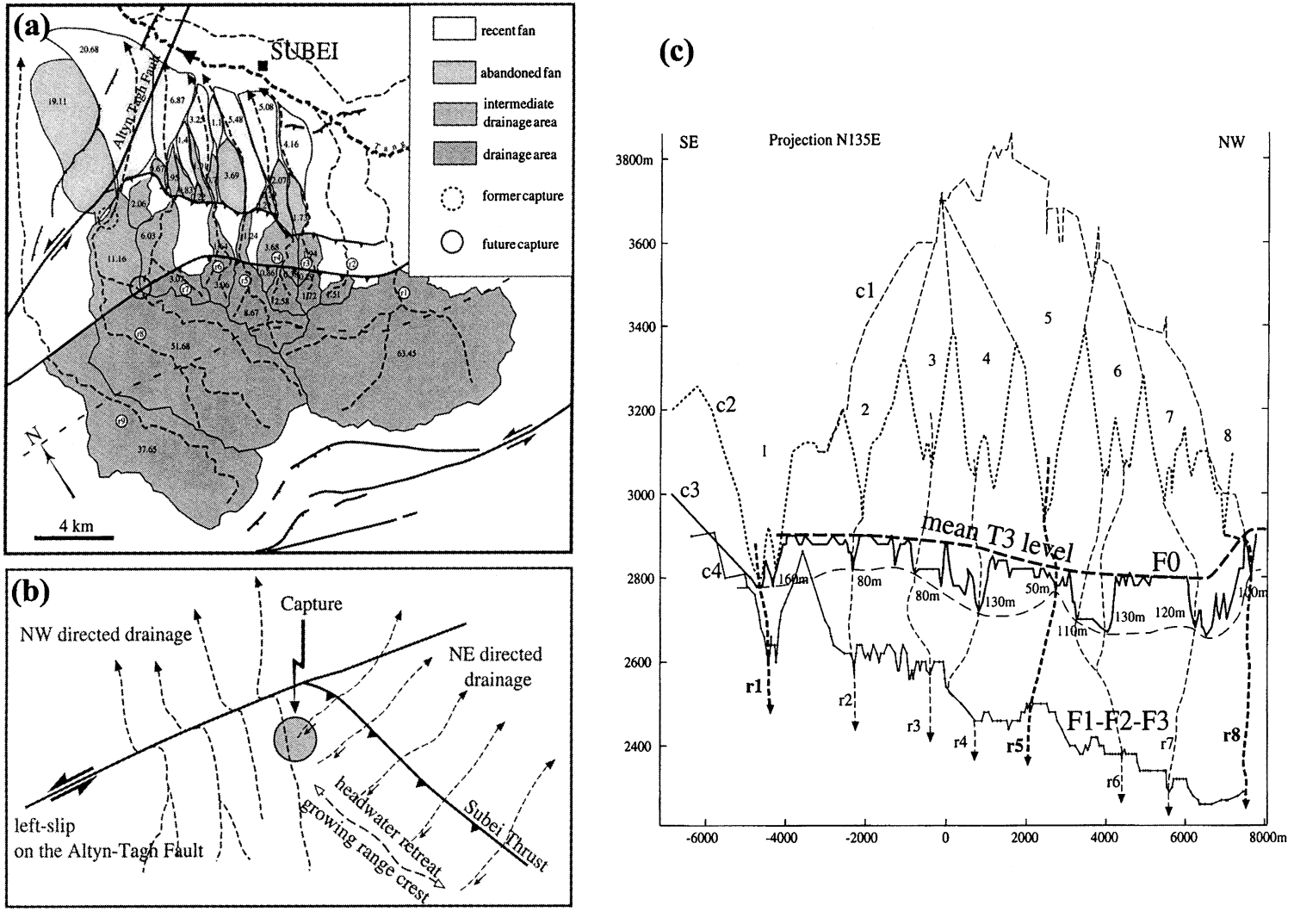

Figure 20. (a) Catchment of main streams and corresponding fan areas. Main faults and thrusts are indicated. (b) Headwater retreat guided by tectonic uplift on Subei thrust lead to capture of northwest flowing streams. (c) Projection of profiles levelled along thrust ledge and across drainage at different levels: c4, along F1; c3, along F0; c2 and c1, across catchments.

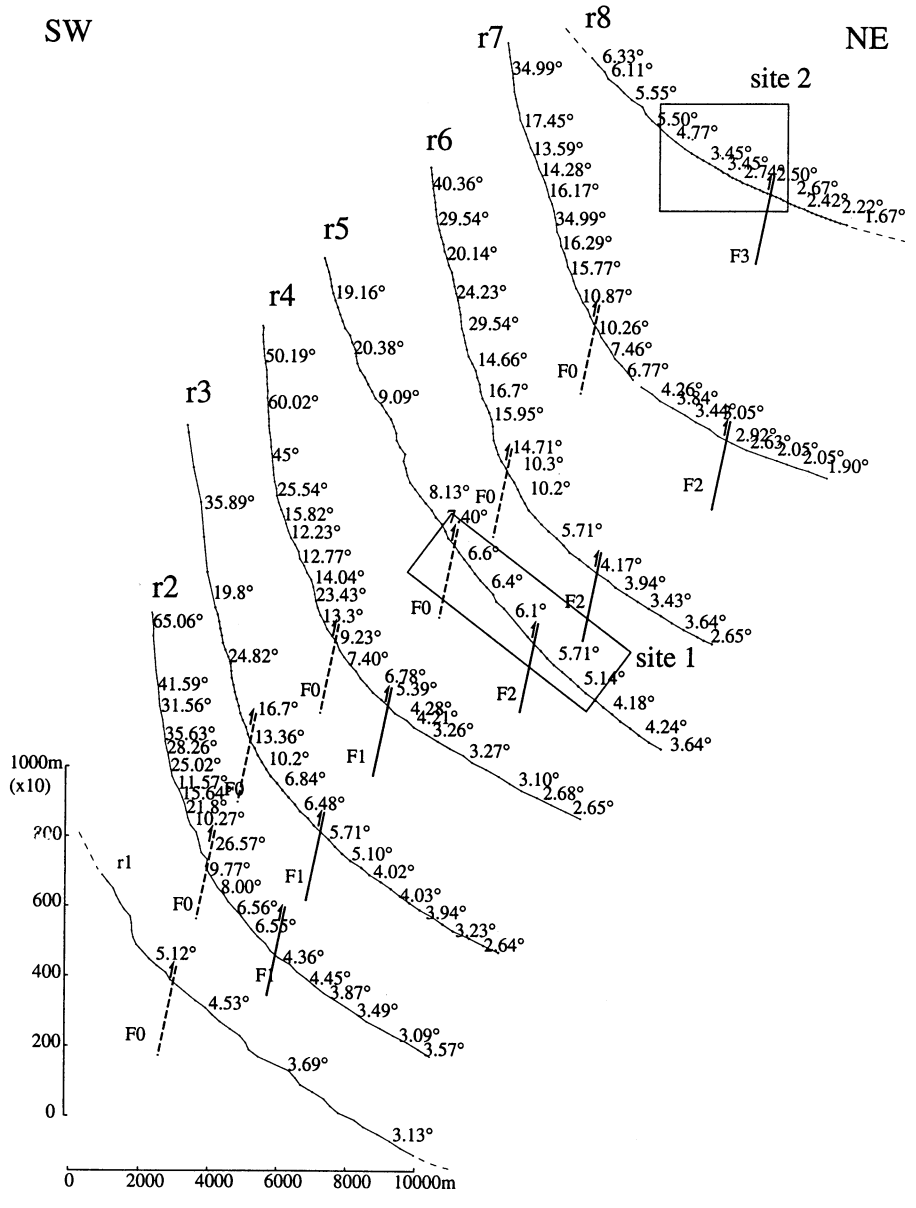

Figure 21. Projection of stream profiles and corresponding slopes.

south of Subei, only the latter two cases are observed. Deeper incision than that required by uplift could not have been driven by the small, 20- to 30-m postglacial base level drop in the Subei basin [*Van der Woerd*, 1998]. Nor could renewed incision due to the more humid, early Holocene optimum [e.g., *Gasse et al.*, 1991; *Liu et al.*, 1998] have had a different effect on only certain streams. Rather, the streambeds of the larger seasonal streams (r5, r8) hang above the bajada slope because their wider, more idle beds across the thrust ledge belong to the part of their course where transport and aggradation are dominant. The shorter, steeper streams, which enter the thrust ledge with full incision power past F0, maintain profile slopes that blend with the slope of the depositional bajada far from the frontal thrust (F1). For these streams, born on the faceted mountain front and flowing perpendicular to it, incision keeps pace with tectonic uplift, which is, in fact, the only driving mechanism of incision.

We conclude that the uplift rate of ~4 mm/yr found at site 1, along r5, and corroborated at site 2, along r8, is the minimum throw rate on the Tanghe Nan Shan thrust (F1-F2). Most likely, the 100- to 130-m (115 ± 15 m) entrenchment of the other streams below T3 is a measure of incision keeping pace with tectonic uplift, and the throw rate is much greater. If T3 were 15,000 to 18,000 years old, consistent with the entrenchments and ages of the lower terraces at site 2 (Figure 12) and the minimum age of T3 at site 1, that rate could be as much as 7.4 ± 2.0 mm/yr. Climate change was a significant factor in shaping the landscape around Subei. Most of the Quaternary deposits along the range

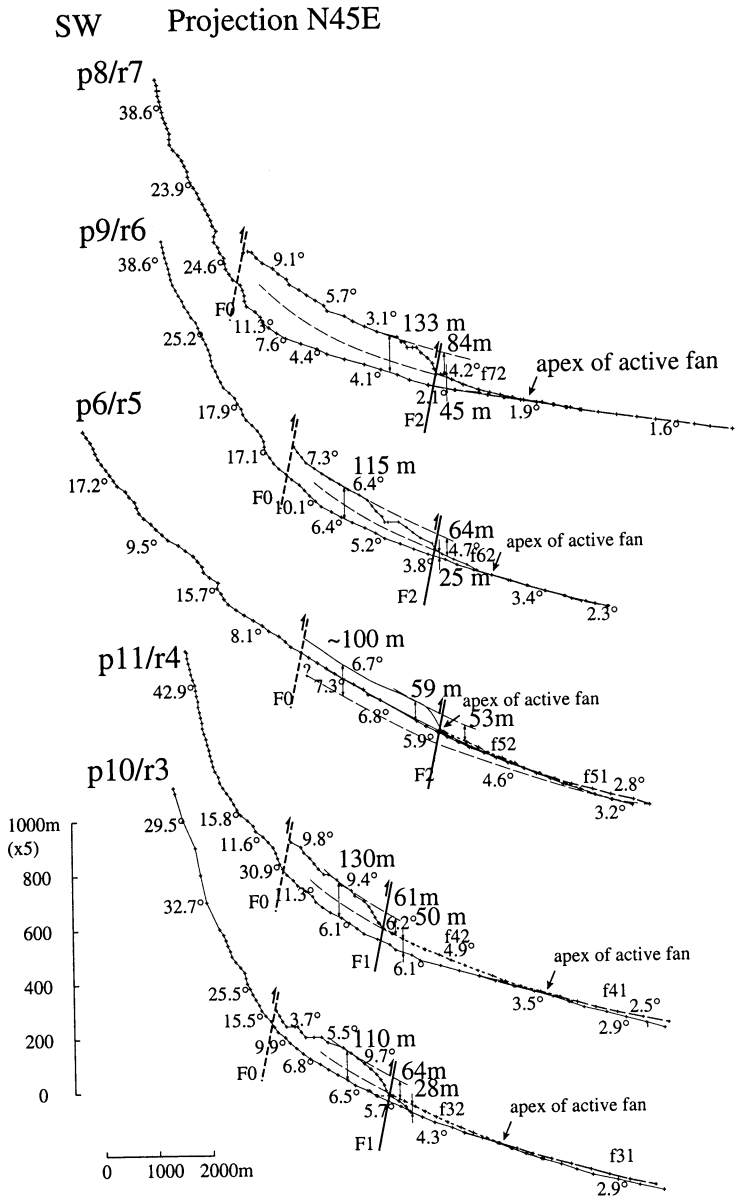

Figure 22. Projection of streams, terrace T3, and fan profiles.

front postdate the LGM. Postglacial warming, accelerating around 14.5 ka, was probably responsible for the emplacement of the most extensive terrace (T3). This was followed by significant aggradation during the early Holocene optimum 9-6 ka [e.g., *Gasse et al.*, 1991; *Liu et al.*, 1998].

The northwestern Tanghe Nan Shan front is a site of rapid shortening and relief growth. With a typical thrust ramp dip of 45°, our results imply differential uplift and N45°E shortening rates of 4 to 7 mm/yr (5.5 ± 1.5 mm/yr). The minimum cumulative shortening of 10 to 12 km across the range front obtained from retrodeformable sections suggests that thrusting began at least $4 \pm 2 \times 10^6$ years ago.

The thrust wedge becomes wider toward the west (Figure 2). The largest section (along r8) may reflect faster north directed migration of thrust splays near the strike-slip fault. Clear triple junctions exist where thrusts F′2 and F3 meet the Altyn Tagh Fault (Figure 2). Such junctions are not stable features and probably evolve with increasing sinistral displacement on the fault and shortening on the thrusts. Nevertheless, the present geometry reflects the instantaneous displacements between the different blocks. Assuming that the faults separate rigid blocks, triangular vector diagrams constrain the way in which such displacements combine (see inset, Plate 1). Slip rate estimates along the Altyn Tagh Fault [*Van der Woerd*, 1998] east and west of the F′2 triple junction are 17 and 22 mm/yr, respectively. The difference between these two rates (~5 mm/yr) is compatible with a shortening rate of 5.5 ± 1.5 mm/yr across F′2. The northeastward decrease in slip rate in-

ferred by several authors [*Peltzer et al.*, 1989; *Meyer et al.*, 1996, 1998; *Van der Woerd*, 1998] along the N70°E striking Altyn Tagh Fault thus probably reflects loss of slip on active thrust splays at successive junctions such as that west of Subei.

Resolution of the vector diagram at the Subei junction also implies that the strike-slip fault east of the thrust should have a more easterly trend (vector AC, inset, Plate 1). Such a change in trend is not observed: the Altyn Tagh Fault keeps striking N70°E across the Subei basin and northwest of it (Figure 1). A component of extension normal to the Altyn Tagh Fault is thus predicted (e, inset, Plate 1) [*Meyer et al.*, 1998]. Such extension is observed northwest of the fault where parallel normal faults cut and offset fan surfaces by tens of meters (Plate 1 and Figures 2 and 10) [*Van der Woerd*, 1998]. The existence of these faults thus concurs to confirm that rigid block kinematics holds for current displacements. It may in fact hold for longer time spans: the presence of the Subei basin, which is a fairly large, hence long-lived, depression along the Altyn Tagh Fault indicates that the junction between the fault and the Tanghe Nan thrust has been in existence for a few million years, probably with a comparable kinematic regime.

Acknowledgments. We thank the China Bureau of Seismology and Institut National des Sciences de l'Univers (INSU, Paris, France) for logistical and financial support. SPOT satellite images were acquired through program Tectoscope, co-sponsored by CNRS and INSU. The Lawrence Livermore National Laboratory (LLNL) group acknowledges support from the Institute of Geophysics and Planetary Physics and the Center for Accelerator Mass Spectrometry at LLNL, operating under the auspices of the U.S. Department of Energy (DOE). Comments by three referees (An Yin, Lothar Ratschbacher, and Wayne Thatcher) helped improve the manuscript. We also acknowledge thoughtful discussions with Stuart Gilder and Chen Yan, who generously let us share insights coming from their magnetostratigraphic work. This is LLNL contribution UCRL-JC-134629 and IPGP contribution 1652.

References

Avouac, J. P., B. Meyer, and P. Tapponnier, On the growth of normal faults and the existence of flats and ramps along the El Asnam active fold and thrust system, *Tectonics, 11*, 1-11, 1992.

Avouac, J. P., P. Tapponnier, M. Bai, H. You and G. Wang, Active thrusting and folding along the northern Tien Shan and late Cenozoic rotation of the Tarim relative to Dzungaria and Kazakhstan, *J. Geophys. Res., 98*, 6755-6804, 1993.

Besse, J., and V. Courtillot, Revised and synthetic apparent polar wander paths of the African, Eurasian, North American, and Indian plates and true polar wander since 200 Ma, *J. Geophys. Res., 96*, 4029-4050, 1991.

Bohlin, B., Oberoligozäne Säugetiere aus dem Shargalteintal (western Kansu), *Paleontol. Sin., 107*, 1-66, 1937.

Bull, W. B., *Geomorphic Responses to Climatic Change*, Oxford Univ. Press, New York, 1991.

Gasse, F., et al., A 13,000-year climate record from western Tibet, *Nature, 353*(6346), 742-745, 1991.

Gaudemer, Y., P. Tapponnier, B. Meyer, G. Peltzer, Guo Shunmin, Chen Zhitai, Dai Huagung and I. Cifuentes, Partitioning of crustal slip between linked, active faults in the eastern Qilian Shan, and evidence for a major seismic gap, the "Tianzhu gap," on the western Haiyuan Fault, Gansu (China), *Geophys. J. Int., 120*, 599-645, 1995.

Ge, S., Bai M., Li Y., Liu G., Zhen Q., Zheng J., and Zhu S., *Active Altyn Fault Zone*, Seismol. Press, Beijing, 1992.

Gilder, S., Chen Yan, and Sevket Sen, Oligo-Miocene magnetostratigraphy and rock magnetism of the Xishuigou-section, Subei (Gansu Province, western China), and implications for shallow inclinations in central Asia, *J. Geophys. Res.*, this issue.

Lasserre, C., et al., Postglacial left slip rate and past occurrence of $M \geq 8$ earthquakes on the western Haiyuan Fault, Gansu, China, *J. Geophys. Res., 104*, 17,633-17,651, 1999.

Lavé, J., and J. P. Avouac, Active folding of fluvial terraces across the Siwaliks Hills, Himalayas of central Nepal, *J. Geophys. Res., 105*, 5735-5770, 2000.

Liu, K., Z. Yao, and L. G. Thompson, A pollen record of Holocene climatic changes from the Dunde ice cap, Qinghai-Tibetan plateau, *Geology, 26*, 135-138, 1998.

Métivier, F., Y. Gaudemer, P. Tapponnier, and B. Meyer, Northeastward growth of the Tibet plateau deduced from balanced reconstruction of two depositional areas: the Qaidam and Hexi corridor basins, China, *Tectonics, 17*, 823-842, 1998.

Meyer, B., Mécanismes des grands tremblements de terre et du raccourcissement crustal oblique au bord nord-est du Tibet, Ph.D. thesis, Univ. Paris VI, Paris, 1991.

Meyer, B., P. Tapponnier, Y. Gaudemer, G. Peltzer, S. Guo, and Z. Chen, Rate of left-lateral movement along the easternmost segment of the Altyn Tagh Fault, east of 96°E (China), *Geophys. J. Int., 124*, 29-44, 1996.

Meyer, B., P. Tapponnier, L. Bourjot, F. Métivier, Y. Gaudemer, G. Peltzer, G. Shunmin and C. Zhitai, Mechanisms of active crustal thickening in Gansu-Qinghai, and oblique, strike-slip controlled, northeastward growth of the Tibet plateau, *Geophys. J. Int., 135*, 1-47, 1998.

Molnar, P., and H. Lyon-Caen, Fault plane solutions of earthquakes and active tectonics of the Tibetan plateau and its margins, *Geophys. J. Int., 99*, 123-153, 1989.

Peltzer, G., P. Tapponnier, Y. Gaudemer, B. Meyer, Guo Shunmin, Yin Kelun, Chen Zhitai and Dai Huagung, Offsets of late Quaternary morphology, rate of slip, and recurrence of large earthquakes on the Chang Ma Fault (Gansu, China), *J. Geophys. Res., 93*, 7793-7812, 1988.

Peltzer, G., P. Tapponnier, and R. Armijo, Magnitude of late Quaternary left-lateral displacements along the north edge of Tibet, *Science, 246*, 1285-1289, 1989.

Regional Geology of Gansu Province, Beijing Publishing House, Beijing, 1989.

Rockwell, T. K., E. A. Keller, and G. R. Dembroff, Quaternary rate of folding of the Ventura Avenue Anticline, western Transverse Ranges, southern California, *Geol. Soc. Am. Bull., 100*, 850-858, 1988.

Rumelhart, P. E., An Yin, E. Cowgill, R. Butler, Z. Qing, and X. F. Wang, Cenozoic vertical axis rotation of the Altyn Tagh fault system, *Geology, 27*, 819-822, 1999.

Stein, R., and G. Ekström, Seismicity and geometry of a 110-km-long blind thrust fault, 2, Synthesis of the 1982-1985 California earthquake sequence, *J. Geophys. Res., 97*, 4865-4883, 1992.

Stuiver, M., and H. A. Polach, Discussion: Reporting of ^{14}C data, *Radiocarbon, 19*, 355-363, 1977.

Stuiver, M., and P. J. Reimer, Extended ^{14}C data base and revised CALIB 3.0 ^{14}C age calibration program, *Radiocarbon, 35*, 215-230, 1993.

Suppe, J., Geometry and kinematics of fault-bend folding, *Am. J. Sci., 283*, 684-721, 1983.

Tapponnier, P., and P. Molnar, Active faulting and tectonics in China, *J. Geophys. Res., 82*, 2905-2930, 1977.

Tapponnier, P., et al., Active thrusting and folding in the Qinlian Shan, and decoupling between upper crust and mantle in northeastern Tibet, *Earth Planet. Sci. Lett., 97*, 382-403, 1990.

Van Der Woerd, J., Couplage cinématique entre décrochements et chevauchements actifs dans le nord du Tibet. Croissance du plateau Tibétain, Ph.D. thesis, 438 pp., Univ. Paris VII, Paris, 1998.

Van Der Woerd, J., F. J. Ryerson, P. Tapponnier, Y. Gaudemer, R. Finkel, A. S. Mériaux, M. Caffee, Zhao Guoguang, and He Qunlu, Holocene left slip-rate determined by cosmogenic surface dating on the Xidatan segment of the Kunlun Fault (Qinghai, China), *Geology, 26*, 695-698, 1998.

Wang, E., Displacement and timing along the northern strand of the Altyn Tagh zone, northern Tibet, *Earth Planet. Sci. Lett., 150*, 55-64, 1997.

Weldon, R. J., Late cenozoic geology of Cajon Pass: Implications for tectonics and sedimentation along the San Andreas Fault, Ph.D. thesis, 400pp., Calif. Inst. of Technol., Pasadena, 1986.

Yeats, R. S., Active faults related to folding, *Active Tectonics*, edited by R. E. Wallace, pp. 63-79, Nat. Acad. Press, Washington, D. C., 1986.

Li Haibing and Xu Zhiqin, Institute of Geology, Ministry of Land and Resources, 26 Baiwanzhuang Road, Beijing 100037, People's Republic of China.

A.-S. Mériaux, B. Meyer, and P. Tapponnier, Institut de Physique du Globe de Paris, CNRS UMR 7578, 4 place Jussieu,
75252 Paris Cédex 05, France. (ameriaux@ipgp.jussieu.fr, meyer@ipgp.jussieu.fr, tappon@ipgp.jussieu.fr)

F. J. Ryerson and J. Van der Woerd, Lawrence Livermore National Laboratory, P.O. Box 808, L202, Livermore, CA 94551, USA. (ryerson1@llnl.gov, vanderwoerd2@llnl.gov)

Xu Xiwei, China Seismological Bureau, No. 63, Fuxing Avenue, Beijing 100029, People's Republic of China. (xxiwei@public3.bta.net.cn)

(Received June 30, 2000; revised December 7, 2000; accepted April 4, 2001.)